Atmos. Chem. Phys., 19, 14031–14056, 2019
https://doi.org/10.5194/acp-19-14031-2019

Atmospheric Chemistry and Physics
Open Access
EGU

Is the recovery of stratospheric O_3 speeding up in the Southern Hemisphere? An evaluation from the first IASI decadal record (2008–2017)

Catherine Wespes[1], Daniel Hurtmans[1], Simon Chabrillat[2], Gaétane Ronsmans[1], Cathy Clerbaux[3,1], and Pierre-François Coheur[1]

[1]Université Libre de Bruxelles (ULB), Faculté des Sciences, Chimie Quantique et Photophysique, Bruxelles, Belgium
[2]Belgian Institute for Space Aeronomy, Brussels, Belgium
[3]LATMOS/IPSL, Sorbonne Université, UVSQ, CNRS, Paris, France

Correspondence: Catherine Wespes (cwespes@ulb.ac.be)

Received: 1 March 2019 – Discussion started: 16 April 2019
Revised: 16 September 2019 – Accepted: 19 September 2019 – Published: 21 November 2019

Abstract. In this paper, we present the global fingerprint of recent changes in middle–upper stratosphere (MUSt; < 25 hPa) ozone (O_3) in comparison with lower stratosphere (LSt; 150–25 hPa) O_3 derived from the first 10 years of the IASI/Metop-A satellite measurements (January 2008–December 2017). The IASI instrument provides vertically resolved O_3 profiles with very high spatial and temporal (twice daily) samplings, allowing O_3 changes to be monitored in these two regions of the stratosphere. By applying multivariate regression models with adapted geophysical proxies on daily mean O_3 time series, we discriminate anthropogenic trends from various modes of natural variability, such as the El Niño–Southern Oscillation (ENSO). The representativeness of the O_3 response to its natural drivers is first examined. One important finding relies on a pronounced contrast between a positive LSt O_3 response to ENSO in the extratropics and a negative one in the tropics, with a delay of 3 months, which supports a stratospheric pathway for the ENSO influence on lower stratospheric and tropospheric O_3. In terms of trends, we find an unequivocal O_3 recovery from the available period of measurements in winter–spring at middle to high latitudes for the two stratospheric layers sounded by IASI ($>\sim 35°$ N–S in the MUSt and $>\sim 45°$ S in the LSt) as well as in the total columns at southern latitudes ($>\sim 45°$ S) where the increase reaches its maximum. These results confirm the effectiveness of the Montreal Protocol and its amendments and represent the first detection of a significant recovery of O_3 concurrently in the lower, in the middle–upper stratosphere and in the total column from one single satellite dataset. A significant decline in O_3 at northern mid-latitudes in the LSt is also detected, especially in winter–spring of the Northern Hemisphere. Given counteracting trends in the LSt and MUSt at these latitudes, the decline is not categorical in total O_3. When freezing the regression coefficients determined for each natural driver over the whole IASI period but adjusting a trend, we calculate a significant speeding up in the O_3 response to the decline of O_3-depleting substances (ODSs) in the total column, in the LSt and, to a lesser extent, in the MUSt, at high southern latitudes over the year. Results also show a small significant acceleration of the O_3 decline at northern mid-latitudes in the LSt and in the total column over the last few years. That, specifically, needs urgent investigation to identify its exact origin and apprehend its impact on climate change. Additional years of IASI measurements would, however, be required to confirm the O_3 change rates observed in the stratospheric layers over the last few years.

1 Introduction

Ozone is a key radiatively active gas of the Earth's atmosphere, in both the troposphere and the stratosphere. While in the troposphere O_3 acts as a strong pollutant and an important greenhouse gas, in the stratosphere and, more particularly, in the middle–low stratosphere, it forms a protective layer for life on Earth against harmful solar radiation. In the

1980s, the scientific community motivated decision-makers to regulate the use of chlorofluorocarbons (CFCs), after the unexpected discovery of the springtime Antarctic ozone hole (Chubachi, 1984; Farman et al., 1985) that was suspected to be induced by continued use of CFCs (Molina and Rowland, 1974; Crutzen, 1974). The O_3 depletion was later verified from measurements at other Antarctic sites (e.g. Farmer et al., 1987) and from satellite observations (Stolarski et al., 1986) and explained by the role of CFCs on the massive destruction of O_3 following heterogeneous reactions on the surface of polar stratospheric clouds (Solomon, 1999; Solomon et al., 1986, and references therein). The world's nations reacted to that human-caused worldwide problem by ratifying the International Vienna Convention for the Protection of the Ozone Layer in 1985 and the Montreal Protocol in 1987 with its later amendments, which forced the progressive banning of these ozone-depleting substances (ODSs) in industrial applications by the early 1990s with a total phase-out of the most harmful CFCs by the year 2000.

A recovery from O_3 depletion is expected in response to the Montreal Protocol and its amendments, but with a delayed period due to the long residence time of halocarbons in the atmosphere (Hofmann et al., 1997; Dhomse el al., 2006; WMO, 2007, 2011). The decline of CFCs in the stratosphere was only initiated about 10 years after their phasing out (Anderson et al., 2000; Newman et al., 2006; Solomon et al., 2006; Mäder et al., 2010; WMO, 2011, 2014). The early signs of ozone response to that decline were identified in several studies that reported first a slowdown in stratospheric ozone depletion (e.g. Newchurch et al., 2003; Yang et al., 2008), followed by a leveling off of upper stratospheric (e.g. WMO, 2007) and total O_3 (e.g. WMO, 2011; Shepherd et al., 2014) depletion since the 2000s. A significant onset of recovery was identified later for upper stratospheric O_3 (e.g. WMO, 2014, 2018; Harris et al., 2015). Only a few studies have shown evidence for increasing total column O_3 in polar regions during springtime (e.g. Salby et al., 2011; Kuttippurath et al., 2013; Shepherd et al., 2014; Solomon et al., 2016). Statistically significant long-term recovery in the total O_3 column (TOC) on a global scale has not yet been observed, likely because of counteracting trends in the different vertical atmospheric layers. Ball et al. (2018) have found that a continuing O_3 decline has prevailed in the lower stratosphere since 1998, leading to a slower increase in total O_3 than expected from the effective equivalent stratospheric chlorine (EESC) decrease. However, the reported decline is not reproduced by the state-of-the-art models and its exact reasons are still unknown (Ball et al., 2018). Wargan et al. (2018) and Galytska et al. (2019) recently reported that the decline in the extratropical lower stratosphere and tropical mid-stratosphere is dynamically controlled by variations in the tropical upwelling.

Although recent papers based on observational datasets and statistical approaches agree that we are currently progressing towards an emergence into ozone recovery (e.g. Pawson et al., 2014; Harris et al., 2015; Steinbrecht et al., 2017; Sofieva et al., 2017; Ball et al., 2018; Weber et al., 2018), trend magnitude and trend significance over the whole stratosphere substantially differ from one study to another and, consequently, they are still subject to uncertainty (Keeble et al., 2018). A clear identification of the onset of O_3 recovery is very difficult due to concurrent sources of O_3 fluctuations (e.g. Reinsel et al., 2005; WMO, 2007, 2011). They include changes in solar ultraviolet irradiance, in atmospheric circulation patterns such as the quasi-biennial oscillation (QBO; Baldwin et al., 2001) and the El Niño–Southern Oscillation (ENSO; e.g. Randel et al., 2009), in temperature, in ODS emissions, and in volcanic eruptions (e.g. Mt Pinatubo in 1991 and Calbuco in 2015) with their feedbacks on stratospheric temperature and dynamics (e.g. Jonsson et al., 2004). Furthermore, the differences in vertical and spatial resolution and in retrieval methodologies (inducing biases), possible instrumental degradations (inducing drifts), and use of merged datasets into composites likely explain part of the trend divergence between various studies. If merging performed on deseasonalized anomalies offers the advantage of removing instrumental biases between the individual data records (Sofieva et al., 2017), large differences remain in anomaly values between the independent datasets, as well as large instrumental drifts and drift uncertainty estimates that prevent statistically accurate trends from being derived (Harris et al., 2015; Hubert et al., 2016). In this context, there is a pressing need for a long-duration, high-density and homogenized O_3 profile dataset to assess significant O_3 changes in different parts of the stratosphere and their contributions to the total O_3.

In this paper, we exploit the high frequency (daily) and spatial coverage of the IASI satellite dataset over the first decade of the mission (January 2008–December 2017) to determine global patterns of reliable trends in the stratospheric O_3 records, separately in the middle–upper stratosphere (MUSt) and the lower stratosphere (LSt). This study is built on previous analysis of stratospheric O_3 trends from IASI, estimated on latitudinal averages over a shorter period (2008–2013) (Wespes et al., 2016). A multivariate linear regression (MLR) model (annual and seasonal formulations) that is similar to that previously used for tropospheric O_3 studies from IASI (Wespes et al., 2017, 2018), but adapted here for the stratosphere with appropriate drivers, is applied to gridded daily mean O_3 time series in the MUSt and the LSt. The MLR model is evaluated in terms of its performance and its ability to capture the observed variability in Sect. 2, in terms of representativeness of O_3 drivers in Sect. 3 and in terms of adjusted trends in Sect. 4. The minimum number of years of IASI measurements that is required to indeed detect the adjusted trends from MLR in the two layers is also estimated in Sect. 4, which ends with an evaluation of the trends detectable in polar winter and spring and with an evaluation of a speeding up in the O_3 changes.

2 Dataset and methodology

2.1 IASI O_3 data

The Infrared Atmospheric Sounding Interferometer (IASI) is a nadir-viewing Fourier transform spectrometer designed to measure the thermal infrared emission of the Earth–atmosphere system between 645 and 2760 cm^{-1}. Measurements are taken from the polar sun-synchronous orbiting meteorological Metop series of satellites, every 50 km along the track of the satellite at nadir and over a swath of 2200 km across the track. With more than 14 orbits a day and a field of view of four simultaneous footprints of 12 km at nadir, IASI provides global coverage of the Earth twice a day at about 09:30 and 21:30 mean local solar time.

The Metop program consists of a series of three identical satellites successively launched to ensure homogenous measurements of atmospheric parameters covering more than 15 years. Metop-A and -B were successively launched in October 2006 and September 2012, respectively. The third and last satellite was launched in November 2018 on board Metop-C. In addition to its exceptional spatio-temporal coverage, IASI also provides good spectral resolution and low radiometric noise, which allows the measurement of a series of gas-phase species and aerosols globally (e.g. Clerbaux et al., 2009; Hilton et al., 2012; Clarisse et al., 2019).

In this study, we use the O_3 profiles retrieved by the Fast Optimal Retrievals on Layers for IASI (FORLI-O_3; version 20151001) near-real time processing chain set up at ULB (see Hurtmans et al., 2012, for a description of the retrieval parameters and the FORLI performances). The FORLI algorithm relies on a fast radiative transfer and a retrieval methodology based on the optimal estimation method (Rodgers, 2000), which requires a priori information (a priori profile and associated variance–covariance matrix). The FORLI-O_3 a priori information consists of one single profile and one covariance matrix built from the global Logan–Labow–McPeters climatology (McPeters et al., 2007). The profiles are retrieved on a uniform 1 km vertical grid on 41 layers from surface to 40 km with an extra layer from 40 km to the top of the atmosphere considered at 60 km. Previous characterization of the FORLI-O_3 profiles (Wespes et al., 2016) have demonstrated a good vertical sensitivity of IASI to the O_3 measurement, with up to four independent levels of information on the vertical profile in the troposphere and the stratosphere (MUSt; LSt; upper troposphere-lower stratosphere – UTLS – 300–150 hPa; middle-low troposphere – MLT – below 300 hPa). The two stratospheric layers that show distinctive patterns of O_3 distributions over the IASI decade (Fig. 1a) are characterized by high sensitivity (degree of freedom for signal – DOFS > 0.85; Fig. 1b) and low total retrieval errors ($< 5\,\%$; see Hurtmans et al., 2012, and Wespes et al., 2016). The decorrelation between the MUSt and the LSt is further evidenced in Fig. 1d, which shows low correlation coefficients (< 0.4) between the mean absolute deseasonalized anomalies (as calculated in Wespes et al., 2017) in the two layers (Fig. 1c). Note that the highest correlation coefficients over the Antarctic (~ 0.4) are due to the smaller vertical sensitivity of the IASI measurements over cold surfaces (Clerbaux et al., 2009). The latest validation exercises for the FORLI-O_3 product have demonstrated a high degree of precision with excellent consistency between the measurements taken from the two IASI instruments on Metop-A and -B, as well as a good degree of accuracy with biases lower than 20 % in the stratospheric layers (Boynard et al., 2018; Keppens et al., 2018). Thanks to these good IASI-FORLI performances, large-scale dynamical modes of O_3 variations and long-term O_3 changes can be differentiated in the four retrieved layers (Wespes et al., 2016). The recent validations have, however, reported a drift in the MUSt FORLI-O_3 time series from comparison with O_3 sondes in the Northern Hemisphere (NH) ($\sim 3.53 \pm 3.09$ DU decade^{-1} on average over 2008–2016; Boynard et al., 2018) that was suggested to result from a pronounced discontinuity ("jump") rather than from a progressive change. Further comparisons with CTM simulations from the Belgian Assimilation System for Chemical ObsErvations (BASCOE; Chabrillat et al., 2018; Errera et al., 2019) confirm this jump that occurred on 15 September 2010 over all latitudes (see Fig. S1 of the Supplement). The discontinuity is suspected to result from updates in level-2 temperature data from Eumetsat that are used as inputs into FORLI (see Hurtmans et al., 2012). Hence, the apparent drift reported by Boynard et al. (2018) likely results from the jump rather than from a progressive "instrumental" drift. This is verified by the absence of drift in the O_3 time series after the jump (non-significant drift of -0.38 ± 2.24 DU decade^{-1} on average over October 2010–May 2017; adapted from Boynard et al., 2018). This is in line with the excellent stability of the IASI Level-1 radiances over the full IASI period (Buffet et al., 2016). From the IASI-BASCOE comparisons, the amplitude of the jump has been estimated as lower than 2.0 DU in the 55° S–55° N latitude band and 4.0 DU in the 55–90° latitude band of each hemisphere. The estimated amplitude of the jump is found to be relatively small in comparison to that of the decadal trends derived in Sect. 4; hence, it cannot explain the trend observed in the IASI dataset. Therefore, the jump is not taken into account in the MLR. The jump values will be, however, considered in the discussion of the O_3 trends (Sect. 4).

Finally, the present study only uses the daytime measurements (defined with a solar zenith angle to the sun $< 83°$) from the IASI-A (aboard Metop-A) instrument, which fully covers the first decade of the IASI mission. The daytime measurements are characterized by a higher vertical sensitivity (e.g. Clerbaux et al., 2009). Quality flags developed in previous IASI studies (e.g. Boynard et al., 2018) were applied a posteriori to exclude data with a poor spectral fit, with less reliability or with cloud contamination.

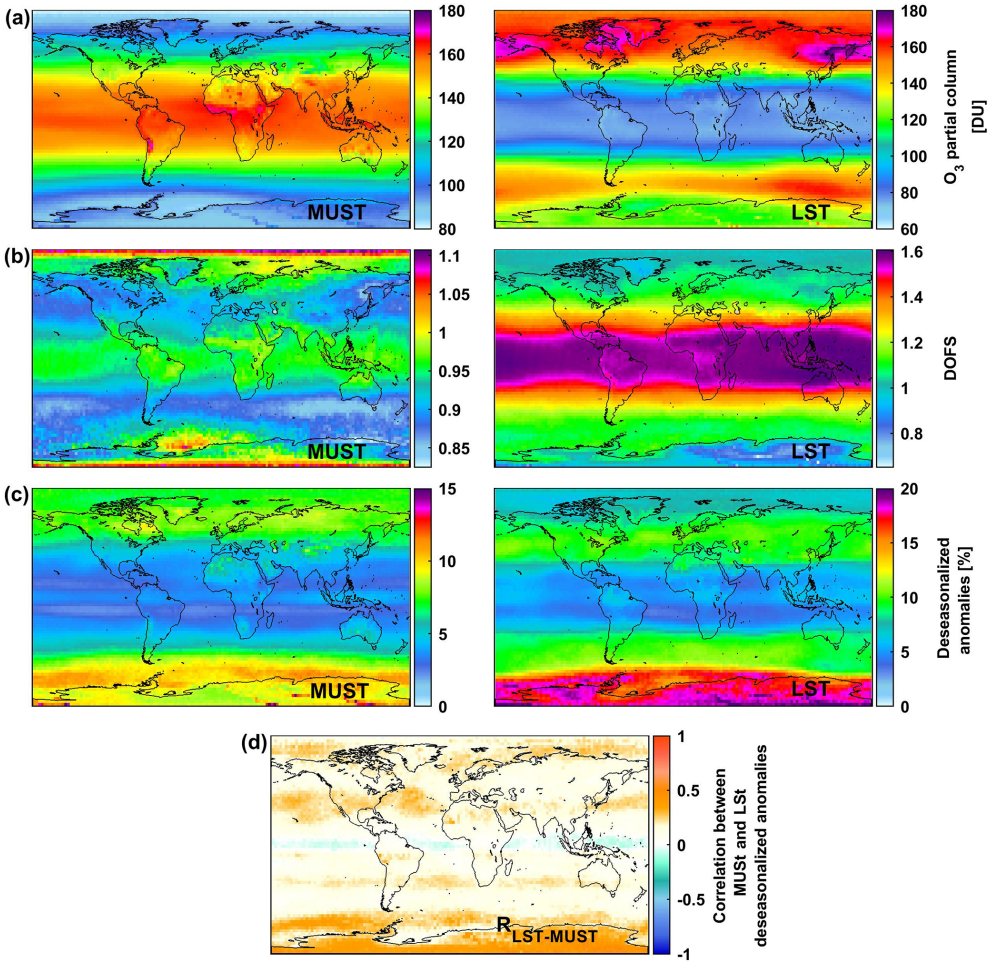

Figure 1. Global distribution of **(a)** daily O_3 columns (in Dobson units – DU), **(b)** associated DOFS, **(c)** absolute deseasonalized anomalies (in percentage) averaged over January 2008–December 2017 in the MUSt (middle–upper stratosphere: > 25 hPa; left panels) and in the LSt (lower stratosphere: 150–25 hPa; right panels). Panel **(d)** shows the correlation coefficients between the daily O_3 deseasonalized anomalies in the MUSt and in the LSt. Note that the scales are different between MUSt and LSt.

2.2 Multivariate regression model

In an effort to unambiguously discriminate anthropogenic trends in O_3 levels from the various modes of natural variability (illustrated globally in Fig. 1c as deseasonalized anomalies), we have applied to the 2.5° × 2.5° gridded daily MUSt and LSt O_3 time series a MLR model that is similar to that previously developed for tropospheric O_3 studies from IASI (see Wespes et al., 2017, 2018) but is here adapted to fit the stratospheric variations:

$$\begin{aligned} O_3(t) = {} & \mathrm{Cst} + x_{j=1} \cdot \boldsymbol{trend} \\ & + \sum\nolimits_{n=1:2} [a_n \cdot \boldsymbol{cos}(n\omega t) + b_n \cdot \boldsymbol{sin}(n\omega t)] \\ & + \sum_{j=2}^{m} x_j X_{\mathrm{norm},j}(t) + \boldsymbol{\varepsilon}(t), \end{aligned} \quad (1)$$

where t is the number of days, x_1 is the trend coefficient in the data, $\omega = 2\pi/365.25$, a_n, b_n, x_j are the regression coefficients of the seasonal and non-seasonal variables, and $\varepsilon(t)$ is the residual variation (assumed to be autoregressive with time lag of 1 d). $X_{\mathrm{norm},j}$ are the m chosen explanatory variables, commonly called "proxies", which are normalized over the study period (2008–2017) with the following:

$$X_{\mathrm{norm}}(t) = 2[X(t) - X_{\mathrm{median}}] / [X_{\max} - X_{\min}]. \quad (2)$$

In addition to harmonic terms that represent the 1-year and 6-month variations, the MLR model includes the anthropogenic O_3 response through a linear trend (LT) term and a set of proxies to parameterize the geophysical processes influencing the abundance of O_3 in the stratosphere. The MLR uses an iterative stepwise backward elimination approach to retain, at the end of the iterations, the most relevant proxies (within a 95 % confidence level) explaining the O_3 variations (e.g. Mäder et al., 2007). Table 1 lists the selected proxies, their sources and their temporal resolutions. The proxies describe the influence of the Quasi-Biennial Oscillation (QBO;

visible from the deseasonalized anomaly maps in Fig. 1c with a typical band-like pattern around the Equator) at 10 and 30 hPa, of the North Atlantic and the Antarctic Oscillations (NAO and AAO), of the ENSO, of the volcanic aerosols (AERO) injected into the stratosphere, of the strength of the Brewer–Dobson circulation (BDC) with the Eliassen–Palm flux (EPF), of the polar O_3 loss driven by the volume of polar stratospheric clouds (VPSC), of the tropopause height variation with the geopotential height (GEO), and of the mixing of tropospheric and stratospheric air masses with the potential vorticity (PV). The main proxies in terms of their influence on O_3 over the period of the IASI mission are illustrated in Fig. 2. The construction of the EPF, VPSC and AERO proxies, which are specifically used in this study, is explained hereafter, while the description of the other proxies can be found in previous IASI studies (Wespes et al., 2016, 2017).

The EPF proxy consists of the normalized upward component of the EP flux crossing 100 hPa and spatially averaged over the 45–75° latitude band for each hemisphere. The fluxes are calculated from the NCEP/NCAR 2.5° × 2.5° gridded daily reanalysis (Kalnay et al., 1996) over the IASI decade. The VPSC proxy is based on the potential volume of PSCs given by the volume of air below the formation temperature of nitric acid trihydrate (NAT) over 60–90° north and south and calculated from the ERA-Interim reanalysis and from the MLS climatology of nitric acid (Ingo Wohltmann, personal communication, 2018; Wohltmann et al., 2007; and references therein). The PSC volume is multiplied by the EESC to account for the changes in the amount of inorganic stratospheric chlorine that activates the polar ozone loss. The O_3 build-up and the polar O_3 loss are highly correlated with wintertime accumulated EP flux and PSC volume, respectively (Fusco and Salby, 1999; Randel et al., 2002; Fioletov and Shepherd, 2003; Rex et al., 2004). These cumulative EP flux and PSC effects on O_3 levels are taken into account by integrating the EPF and VPSC proxies over time with a specific exponential decay time according to the formalism of Brunner et al. (2006; see Eq. 4). We set the relaxation timescale to 3 months everywhere, except during the wintertime build-up phase of O_3 in the extratropics (from October to March in the NH and from April to September in the Southern Hemisphere – SH) when it is set to 12 months. For EPF, it accounts for the slower relaxation time of extratropical O_3 in winter due to its longer photochemical lifetime. For VPSC, the 12-month relaxation time accounts for a stronger effect of stratospheric chorine on spring O_3 levels: the maximum of the accumulated VPSC (Fig. 2) coincides with the maximum extent of the O_3 hole that develops during springtime and that lasts until November. Note that correlations between VPSC and EPF are possible since the same method is used to build these cumulative proxies. VPSC and EPF are also dynamically anti-correlated to some extent since a strong BDC is connected with warm polar stratospheric temperatures and, hence, reduced PSC volume (e.g. Wohltmann et al., 2007).

The AERO proxy is derived from the aerosol optical depth (AOD) of sulfuric acid only. That proxy consists of latitudinally averaged (22.5–90° N: AERO-N; 22.5–90° S: AERO-S; and 22.5° S–22.5° N: AERO-Eq) extinction coefficients at 12 µm calculated from merged aerosol datasets (SAGE, SAM, CALIPSO, OSIRIS, 2-D model simulation and Photometer; Thomason et al., 2018) and vertically integrated over the two IASI stratospheric O_3 columns (AERO-MUSt and AERO-LSt). Figure 2 shows the AERO proxies (AERO-N, AERO-S and AERO-Eq) corresponding to the AOD over the whole stratosphere (150–2 hPa), while Fig. 3 represents the latitudinal distribution of the volcanic sulfuric acid extinction coefficients integrated over the whole stratosphere (a) and, separately, over the MUSt (b) and the LSt (c) from 2005 to 2017. The AOD distributions indicate the need for considering one specific AERO proxy for each latitudinal band (AERO-N, AERO-S and AERO-Eq) and for each vertical layer (AERO-MUSt and AERO-LSt). Note that, as an alternative proxy to AERO, the surface area density of ambient aerosol, which represents the aerosol surface available for chemical reactions, has been tested, giving similar results.

Note also that, similarly to what has already been found for tropospheric O_3 from IASI (Wespes et al., 2016), several time lags for ENSO (1-, 3- and 5-month lags; namely, ENSO-lag1, ENSO-lag3 and ENSO-lag5) are also included in the MLR model to account for a possible delay in the O_3 response to ENSO at high latitudes.

Finally, autocorrelation in the noise residual $\varepsilon(t)$ (see Eq. 1 in Wespes et al., 2016) is accounted for in the MLR analysis with time lag of one day to yield the correct estimated standard errors for the regression coefficients. They are estimated from the covariance matrix of the regression coefficients and corrected at the end of the iterative process by the autocorrelation of the noise residual. The regression coefficients are considered significant if they fall in the 95 % confidence level (defined by 2σ level).

In the seasonal formulation of the MLR model, the main proxies ($x_j \boldsymbol{X}_{\mathrm{norm},j}$; with x_j, the regression coefficient, and $X_{\mathrm{norm},j}$, the normalized proxy) are split into four seasonal functions $(x_{\mathrm{spr}}\boldsymbol{X}_{\mathrm{norm,spr}} + x_{\mathrm{sum}}\boldsymbol{X}_{\mathrm{norm,sum}} + x_{\mathrm{fall}}\boldsymbol{X}_{\mathrm{norm,fall}} + x_{\mathrm{wint}}\boldsymbol{X}_{\mathrm{norm,wint}})$ that are independently and simultaneously adjusted for each grid cell (Wespes et al., 2017). Hence, the seasonal MLR adjusts four coefficients (instead of one in the annual MLR) to account for the seasonal O_3 response to changes in the proxy. If that method avoids over-constraining the adjustment by the year-round proxies and, hence, reduces the systematic errors, the smaller daily data points covered by the seasonal proxies translate to a lower significance of these proxies. This is particularly true for EPF and VPSC, which compensate each other by construction. As a consequence, the annual MLR is performed first in this study and then complemented with the seasonal one when it is found helpful for further interpreting the observations.

Figure 4 shows the latitudinal distributions of the O_3 columns in the two stratospheric layers over the IASI decade

Table 1. List of the explanatory variables used in the multi-linear regression model applied on IASI stratospheric O_3, their temporal resolution and their sources.

Proxy	Description (*resolution*)	Sources (last access: 2 November 2019)
F10.7	The 10.7 cm solar radio flux (*daily*)	NOAA National Weather Service Climate Prediction Center: ftp://ftp.ngdc.noaa.gov/STP/space-weather/solar-data/solar-features/solar-radio/noontime-flux/penticton/penticton_adjusted/listings/listing_drao_noontime-flux-adjusted_daily.txt
$QBO^{10}QBO^{30}$	Quasi-Biennial Oscillation index at 10 and 30 hPa (*monthly*)	Free University of Berlin: https://www.geo.fu-berlin.de/en/met/ag/strat/produkte/qbo/
EPF	Vertical component of Eliassen–Palm flux crossing 100 hPa, averaged over 45–75° for each hemisphere and accumulated over the last 3 or 12 months depending on the time period and the latitude (see text for more details) (*daily*)	Calculated at ULB from the NCEP/NCAR gridded reanalysis: https://www.esrl.noaa.gov/psd/data/gridded/data.ncep.reanalysis.html
AERO	Stratospheric volcanic aerosols; vertically integrated sulfuric acid extinction coefficient at 12 µm over 150–25 and 25–2 hPa, averaged over the tropics and the extratropics north and south (see text for more details) (*monthly*)	Extinction coefficients processed at the Institute for Atmosphere and Climate (ETH Zurich, Switzerland; Thomason et al., 2018)
VPSC	Volume of polar stratospheric clouds for the NH and the SH multiplied by the equivalent effective stratospheric chlorine (EESC) and accumulated over the last 3 or 12 months (see text for details) (*daily*)	Processed at the Alfred Wagner Institute (AWI, Postdam, Germany; Ingo Wohltmann, personal communication, 2018) EESC taken from the Goddard Space Flight Center: https://acd-ext.gsfc.nasa.gov/Data_services/automailer/index.html
ENSO	Multivariate El Niño–Southern Oscillation Index (MEI) (*2-monthly averages*)	NOAA National Weather Service Climate Prediction Center: https://www.esrl.noaa.gov/psd/enso/mei/
NAO	North Atlantic Oscillation index for the NH (*daily*)	ftp://ftp.cpc.ncep.noaa.gov/cwlinks/norm.daily.nao.index.b500101.current.ascii
AAO	Antarctic Oscillation index for the SH (*daily*)	ftp://ftp.cpc.ncep.noaa.gov/cwlinks/norm.daily.aao.index.b790101.current.ascii
GEO PV	Geopotential height at 200 hPa ($2.5° \times 2.5°$ gridded) (*daily*) Potential vorticity at 200 hPa ($2.5° \times 2.5°$ gridded) (*daily*)	http://apps.ecmwf.int/datasets/data/interim-full-daily/?levtype=pl

(first panels in Fig. 4a and b), as well as those simulated by the annual MLR regression model (second panels) along with the regression residuals (third panels). The root mean square error (RMSE) of the regression residual and the contribution of the MLR model to the IASI O_3 variations (calculated as $\frac{\sigma\left(\boldsymbol{O}_3^{\text{Fitted\_model}}(t)\right)}{\sigma(\boldsymbol{O}_3(t))}$, where σ is the standard deviation relative to the regression model and to the IASI time series; bottom panels) are also represented (bottom panels). The results indicate that the model reproduces ∼ 25 %–85 % and ∼ 35 %–95 % of the daily O_3 variations captured by IASI in the MUSt and the LSt, respectively, with the best representation in the tropics and the worst around the SH polar vortex, and that the residual errors are generally lower than 10 % everywhere for the two layers, except for the spring O_3 hole region in the LSt. The RMSE relative to the IASI O_3 time series are lower than 15 and 20 DU at global scale in the MUSt and the LSt, respectively, except around the SH polar vortex in the LSt (∼ 30 DU). On a seasonal basis (figure not shown), the results are only slightly improved: the model explains ∼ 35 %–90 % and ∼ 45 %–95 % of the annual variations and the RMSEs are lower than ∼ 12 and ∼ 23 DU everywhere, in the MUSt and the LSt, respectively. These results verify that the MLR models (annual and seasonal) reproduce well the time evolution of O_3 over the IASI decade in the two stratospheric

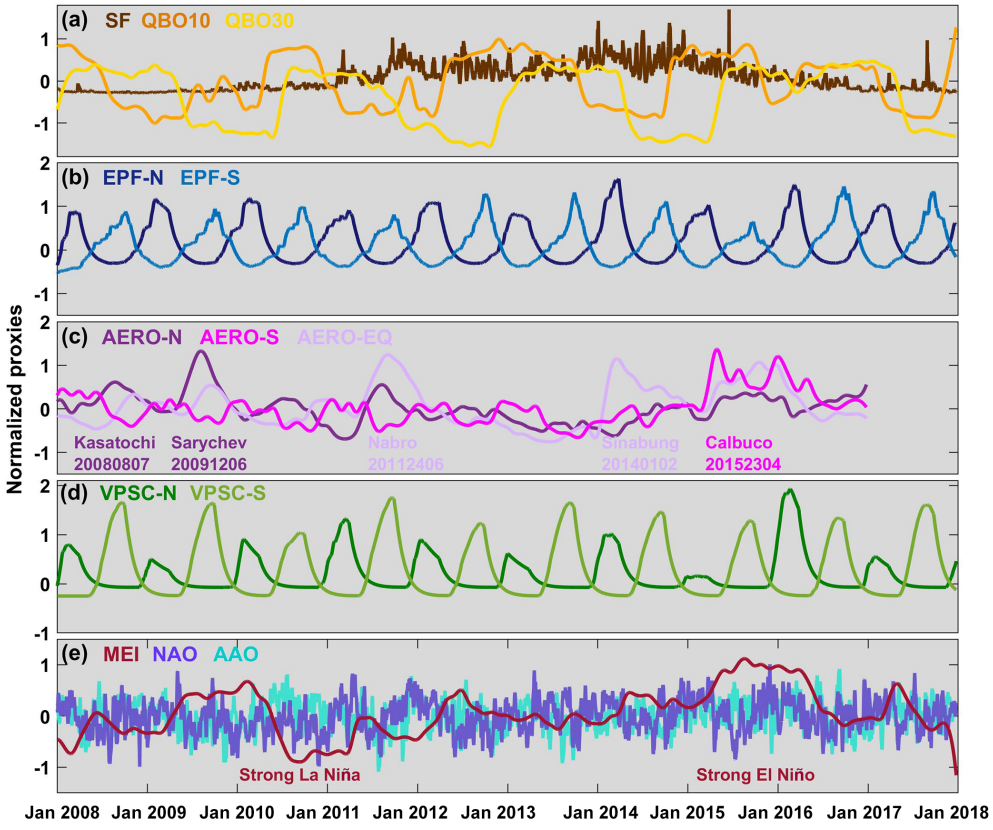

Figure 2. Normalized proxies as a function of time for the period covering January 2008 to December 2017 for **(a)** the F10.7 cm solar radio flux (SF) and the equatorial winds at 10 (QBO10) and 30 hPa (QBO30), respectively; **(b)** the upward components of the EP flux crossing 100 hPa accumulated over time and averaged over the 45–75° latitude band for each hemispheres (EPF-N and EPF-S); **(c)** the extinction coefficients at 12 µm vertically integrated over the stratospheric O_3 column (from 150–2 hPa) and averaged over the extratropics north and south (22.5–90° N–S; AERO-N and AERO-S) and over the tropics (22.5° S–22.5° N; AERO-EQ) (the main volcanic eruptions are indicated); **(d)** the volume of polar stratospheric clouds multiplied by the equivalent effective stratospheric chlorine (EESC) and accumulated over time for the Northern and Southern Hemispheres (VPSC-N and VPSC-S); and **(e)** the El Niño–Southern Oscillation (ENSO), North Atlantic (NAO) and Antarctic (AAO) oscillations.

layers and, hence, that they can be used to identify and quantify the main O_3 drivers in these two layers (see Sect. 3).

The MLR model has also been tested on nighttime FORLI-O_3 measurements only and simultaneously with daytime measurements, but this resulted in a lower-quality fit, especially in the MUSt over the polar regions. This is due to the smaller vertical sensitivity of IASI during nighttime measurements, especially over cold surfaces, which causes larger correlations between stratospheric and tropospheric layers (e.g. 40 %–60 % at high northern latitudes versus ∼ 10 %–20 % for daytime measurements based on deseasonalized anomalies) and, hence, which mixes counteracting processes from these two layers. For this reason, only the results for the MLR performed on daytime measurements are presented in this paper.

3 Drivers of O_3 natural variations

Ascribing a recovery in stratospheric O_3 to a decline in stratospheric halogen species requires first identifying and quantifying natural cycles that may produce trend-like segments in the O_3 time series, in order to prevent any misinterpretation of those segments as signs of O_3 recovery. The MLR analysis performed in Sect. 2.2 that was found to give a good representation of the MUSt and LSt O_3 records shows distinctive relevant patterns for the individual proxies retained in the regression procedure, as represented in Fig. 5. The fitted drivers are characterized by significant regional differences in their regression coefficients with regions of in-phase relation (positive coefficients) or out-of-phase relation (negative coefficients) with respect to the IASI stratospheric O_3 anomalies. The areas of significant drivers (in the 95 % confidence limit) are surrounded by non-significant cells when accounting for the autocorrelation in the noise residual. Figure 6a and b, respectively, represent the latitu-

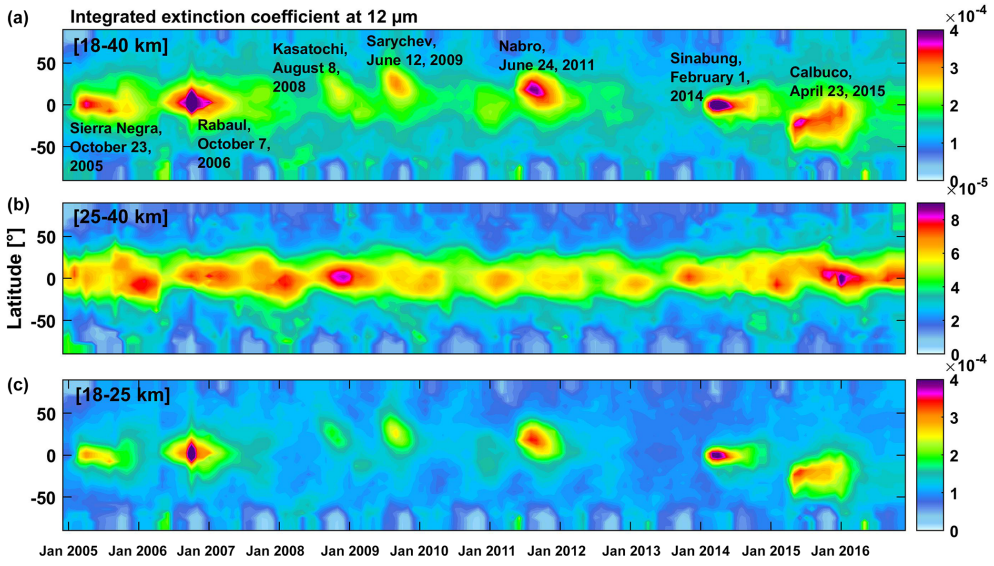

Figure 3. Latitudinal distribution of volcanic sulfuric acid extinction coefficient at 12 µm integrated **(a)** over the stratosphere, **(b)** over the middle stratosphere and **(c)** over the lower stratosphere, as a function of time from 2005 to 2017. The dataset consists of monthly mean aerosol data merged from SAGE, SAM, CALIPSO, OSIRIS, 2-D model simulation and Photometer (processed at NASA Langley Research Center, USA, and ETH Zurich, Switzerland).

dinal averages of the fitted regression coefficients for the significant proxies showing latitudinal variation only in the O_3 response (namely, QBO, EPF, VPSC, AERO and ENSO) and of the contribution of these drivers to the O_3 variability (calculated as the product of the 2σ variability of each proxy by its corresponding fitted coefficient, i.e. the 2σ variability of the reconstructed proxies). The 2σ O_3 variability in the IASI measurements and in the fitted MLR model are also represented (black and grey lines, respectively). Figure 7 displays the same results as Fig. 6b but for the austral spring and winter periods only (using the seasonal MLR).

The PV and GEO proxies are generally minor components (not shown here) with relative contributions smaller than 10 % and large standard errors (> 80 %), except in the tropics where the contribution for GEO reaches 40 % in the LSt due to the tropopause height variation. Each other adjusted proxy (QBO, SF, EPF, VPSC, AERO, ENSO, NAO and AAO) is an important contributor to the O_3 variations, depending on the layer, region, and season as described next:

1. *QBO*. The QBO at 10 and 30 hPa are important contributors around the Equator for the two stratospheric layers. It shows up as a typical band-like pattern of high positive coefficients confined equatorward of ∼ 15° N–S where the QBO is known to be a dominant dynamical modulation force associated with strong convective anomalies (e.g. Randel and Wu, 1996; Tian et al., 2006; Witte et al., 2008). In that latitude band, QBO10 and QBO30 explain up to ∼ 8 and ∼ 5 DU, respectively, of the MUSt and LSt yearly O_3 variations (see Figs. 5 and 6b; i.e. relative contributions up to ∼ 50 % and ∼ 40 % for QBO10/30 in MUSt and LSt O_3, respectively). The QBO is also influencing O_3 variations poleward of 60° N–S with a weaker correlation between O_3 and equatorial wind anomalies as well as in the sub-tropics with an out-of-phase transition. That pole-to-pole QBO influence results from the QBO modulation of extratropical waves and its interaction with the BDC (e.g. Fusco and Salby, 1999). A pronounced seasonal dependence is observed in the out-of-phase subtropical O_3 anomalies in the MUSt, with the highest amplitude oscillating between the hemispheres in their respective winter (∼ 5 DU of O_3 variations explained by QBO10/30 at ∼ 20° S during JJA and at ∼ 20° N during DJF; see Fig. 7b for the JJA period in the MUSt; the DJF period is not shown), which is in agreement with Randel and Wu (1996). The amplitude of the QBO signal is found to be stronger for QBO30 than for QBO10 in the LSt, which is in good agreement with studies from other instruments for the total O_3 (e.g. Baldwin et al., 2001; Steinbrecht et al., 2006; Frossard et al., 2013; Coldewey-Egbers et al., 2014) and from IASI in the troposphere (Wespes et al., 2017). The smaller amplitude of O_3 response to QBO10 in the LSt compared to the MUSt is again in agreement with previous studies that reported changes in the phase of the QBO10 response as a function of altitude with a positive response in the upper stratosphere and destructive interference in the middle–low stratosphere (Chipperfield et al., 1994; Brunner et al., 2006).

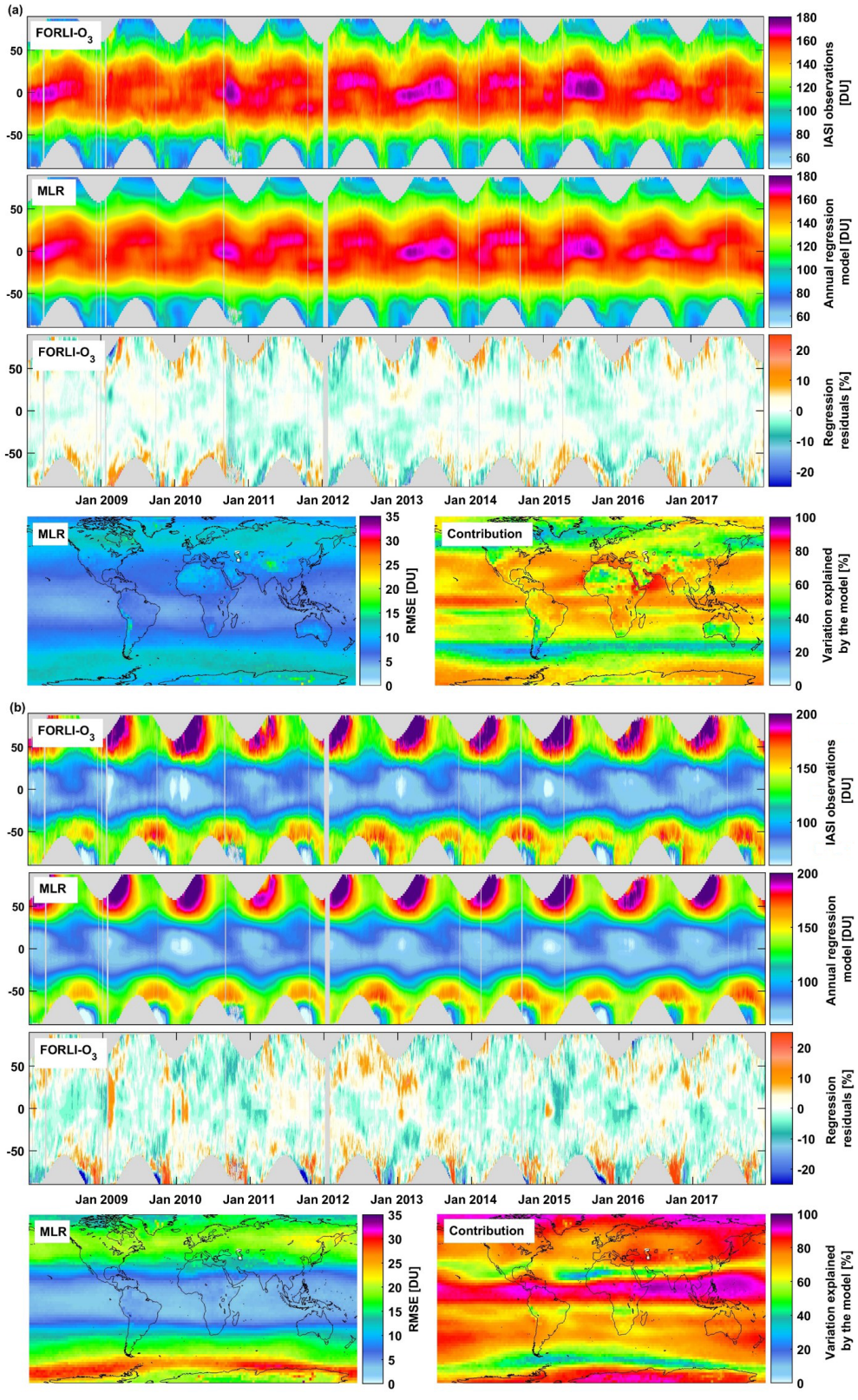

Figure 4. Latitudinal distribution of **(a)** MUSt O_3 column and **(b)** LSt O_3 columns as a function of time observed from IASI (in DU; top panels), simulated by the annual regression model (in DU, second panels) and of the regression residuals (in percentage; third panels). Global distribution of RMSE of the regression residual (in DU) and fraction of the variation in IASI data explained by the regression model calculated as $\left[100 \times \left(\sigma\left(\boldsymbol{O}_3^{\text{Fitted\_model}}(t)\right)/\sigma\left(\boldsymbol{O}_3(t)\right)\right)\right]$ (in percentage; fourth panels).

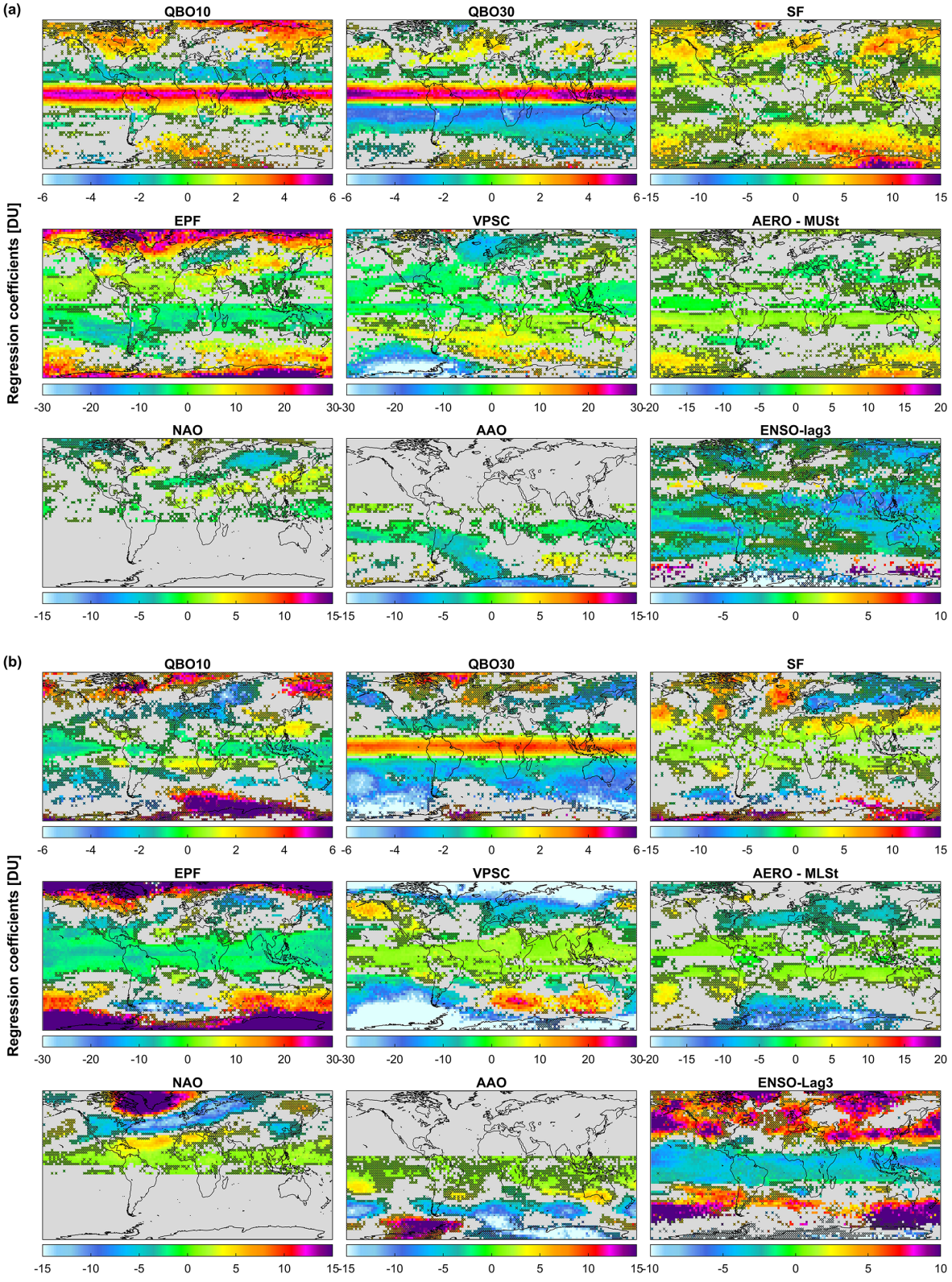

Figure 5. Global distribution of the annual regression coefficient estimates (in DU) for the main O_3 drivers in **(a)** MUSt and in **(b)** LSt: QBO10, QBO30, SF, EPF, VPSC, AERO, NAO, AAO and ENSO (ENSO-lag3 for both LSt and MUSt). Grey areas and crosses refer to non-significant grid cells within the 95 % confidence limit. Note that the scales differ among the drivers.

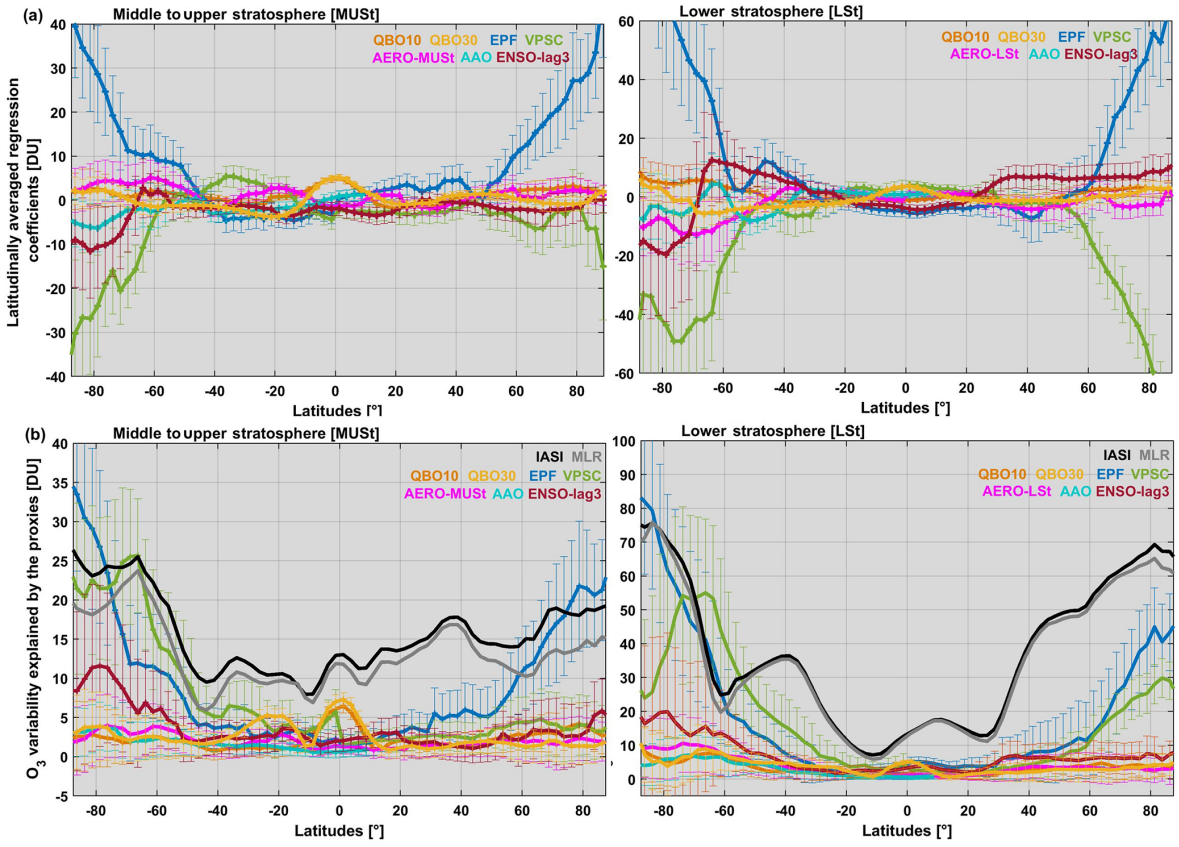

Figure 6. Latitudinal distributions **(a)** of fitting regression coefficients for various O_3 drivers (QBO10, QBO30, EPF, VPSC, AERO, AAO and ENSO-lag3; in DU) and **(b)** of 2σ O_3 variability due to variations in those drivers (in DU) from the annual MLR in MUSt and LSt (left and right panels respectively). Vertical bars correspond **(a)** to the uncertainty of fitting coefficients at the 2σ level and **(b)** to the corresponding error contribution to O_3 variation. Note that the scales are different.

2. *SF.* In the MUSt layer, the solar cycle O_3 response is one of the strongest contributors and explains globally between ~ 2 and 15 DU of in-phase O_3 variations (i.e. higher O_3 values during maximum solar irradiance) with the largest amplitude over the highest latitude regions (see Fig. 5; relative contribution up to $\sim 20\,\%$). The solar influence in the LSt is more complex with regions of in-phase and out-of-phase O_3 variations. The impact of solar variability on stratospheric O_3 abundance is due to a combination of processes: a modification in the O_3 production rates in the upper stratosphere induced by changes in spectral solar irradiance (e.g. Brasseur, 1993), the transport of solar proton event-produced NO_y from the mesosphere down to the middle to low stratosphere where it decreases active chlorine and bromine and, hence, O_3 destruction (e.g. Jackman et al., 2000; Hood and Soukharev, 2006; and references therein) while it enhances the O_3 destruction in the MUSt through NO_x catalysed cycles, and its impact on the lower stratospheric dynamics including the QBO (e.g. Hood et al., 1997; Zerefos et al., 1997; Kodera and Kuroda, 2002; Hood and Soukharev, 2003; Soukharev and Hood, 2006). As for the QBO, the strong SF dependence at polar latitudes in the LSt with zonal asymmetry in the O_3 response reflects the influence of the polar vortex strength and of stratospheric warmings and is in good agreement with previous results (e.g. Hood et al., 1997; Zerefos et al., 1997; Labitzke and van Loon, 2000; Steinbrecht et al., 2003; Coldewey-Egbers et al., 2014). It is also worth noting that because only one solar cycle is covered, the QBO and SF effects could not be completely separated because of their strong interaction (e.g. McCormack et al., 2007; Roscoe and Haigh, 2007; Kuttippurath et al., 2013).

3. *EPF.* The vertical component of the planetary wave Eliassen–Palm flux entering the lower stratosphere corresponds to the divergence of the wave momentum that drives the meridional residual Brewer–Dobson circulation. In agreement with previous studies (e.g. Fusco and Salby, 1999; Randel et al., 2002; Brunner et al., 2006; Weber et al., 2011), fluctuations in the BDC are shown to cause changes to stratospheric O_3 distribution observed from IASI: EPF largely positively con-

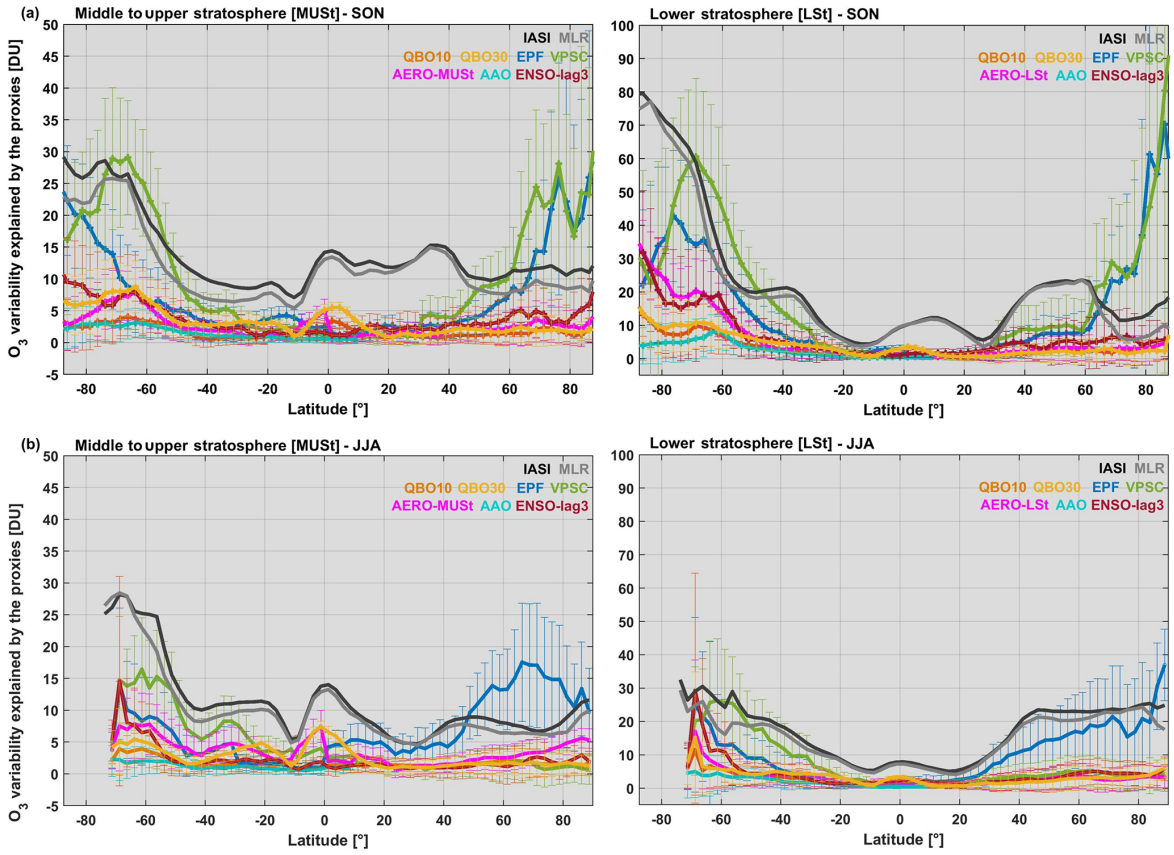

Figure 7. Same as Fig. 6b but for **(a)** the austral winter and **(b)** the austral spring periods (JJA and SON, respectively) from the seasonal MLR. Note that the scales are different.

tributes to the LSt O_3 variations at high latitudes of both hemispheres, where O_3 is accumulated because of its long chemical lifetime, with amplitude ranging between $\sim$ 20 and 100 DU (see Figs. 5 and 6; i.e. relative contribution of $\sim$ 35 %–150 %). The influence of the EPF decreases at lower latitudes where a stronger circulation induces more O_3 transported from the tropics to middle and high latitudes and, hence, a decrease in O_3 levels, particularly below 20 km (Brunner et al., 2006). The influence of EP fluxes in the Arctic is the smallest in summer (see Fig. 7; $<\sim$ 35 DU vs. $\sim$ 70 DU in fall; the two other seasons are not shown) due to the later O_3 build-up in polar vortices. In the SH, because of the formation of the O_3 hole, the EP influence is smaller than in the NH and the seasonal variations are less marked. In the MUSt, the O_3 response attributed to variations in EPF is positive in both hemispheres, with a much lower amplitude than in the LSt (up to $\sim$ 20–35 DU). The region of out-of-phase relation with negative EPF coefficients over the high southern latitudes (Fig. 5b) is likely attributable to the influence of VPSC that has correlations with EPF by construction (see Sect. 2.2). Furthermore, given the annual oscillations in EPF, compensation by the 1-year harmonic term (Eq. 1, Sect. 2) is found, but it remains weaker than the EPF contribution (data not shown), in particular at high latitudes where the EPF contribution is the largest.

4. *VPSC*. Identically to EPF, VPSC is shown to mainly contribute to O_3 variations in the LSt over the polar regions ($\sim$ 55 DU or 40 % in the NH vs. $\sim$ 60 DU or 85 % in the SH on a longitudinal average; see Fig. 6b) but with an opposite phase (Figs. 5 and 6a). The amplitude of the O_3 response to VPSC reaches its maximum over the southern latitudes during the spring ($\sim$ 60 DU; see Fig. 7a for the austral spring period), which is consistent with the role of PSCs on the polar O_3 depletion when there is sufficient sunlight. The strong VPSC influence found at high northern latitudes in fall (Fig. 7a) are due to compensation effects with EPF as pointed out above and verified from sensitivity tests (not shown). Note also that the VPSC contribution to MUSt reflects the larger correlation between the two stratospheric layers over the southern polar region (Sect. 2.1, Fig. 1d).

5. *AERO*. Five important volcanic eruptions with stratospheric impact occurred during the IASI mission

(Kasatochi in 2008, Sarychev in 2009, Nabro in 2011, Sinabung in 2014 and Calbuco in 2015; see Fig. 3). The two major eruptions of the last decades, El Chichon (1982) and Mt Pinatubo (1991), have injected sulfur gases into the stratosphere. They have been shown to enhance PSC particle abundances ($\sim$ 15–25 km altitude), to remove NO_x (through reaction with the surface of the sulfuric aerosol to form nitric acid) and, hence, to make the ozone layer more sensitive to active chlorine (e.g. Hofmann and Solomon, 1989; Hofmann and Oltmans, 1993; Portmann et al., 1996; Solomon et al., 2016). Besides this chemical effect, the volcanic aerosols also warm the stratosphere at lower latitudes through scattering and absorption of solar radiation, which further induces indirect dynamical effects (Dhomse et al., 2015; Revell et al., 2017). Even though the recent eruptions have been of smaller magnitude than El Chichon and Mt Pinatubo, they produced sulfur ejection through the tropopause into the stratosphere (see Sect. 2.2, Figs. 2 and 3), as seen with AOD reaching 5×10^{-4} over the stratosphere (150–2 hPa), especially following the eruptions of Nabro (13.3° N, 41.6° E), Sinabung (3.1° N, 98.3° E) and Calbuco (41.3° S, 72.6° W). In the LSt, the regression supports an enhanced O_3 depletion over the Antarctic in the presence of sulfur gases with a significantly negative annual O_3 response reaching $\sim$ 25 DU (i.e. relative contribution of $\sim$ 20 % into O_3 variation; see Fig. 5b). On the contrary, enhanced O_3 levels in response to sulfuric acid are found in the MUSt with a maximum impact of up to 10 DU (i.e. relative contribution of $\sim$ 20 % into the O_3 variation; see Fig. 5a) over the Antarctic. The change in phase in the O_3 response to AERO between the LSt ($\sim$ 15–25 km) and the MUSt ($\sim$ 25–40 km) over the Antarctic, as well as between polar and lower latitudes in the LSt (see Figs. 5 and 6a), agrees well with the heterogeneous reactions on sulfuric aerosol surface, which reduce the concentration of NO_x to form nitric acid, leading to enhanced O_3 levels above 25 km but leading to decreased O_3 levels due to chlorine activation below 25 km (e.g. Solomon et al., 1996). On a seasonal basis, the depletion due to the presence of sulfur gases reaches $\sim$ 30 DU on a longitudinal average, over the SH polar region during the austral spring (see Fig. 7a), highlighting the link between volcanic gases converted to sulfate aerosols and heterogeneous polar halogen chemistry.

6. *NAO.* The NAO is an important mode of global climate variability, particularly in northern winter. It describes large-scale anomalies in sea level pressure systems between the sub-tropical Atlantic (Azores; high pressure system) and sub-polar (Iceland; low pressure system) regions (Hurrell, 1995). It disturbs the location and intensity of the North Atlantic jet stream that separates these two regions depending on the phase of NAO. The positive (negative) phase of the NAO corresponds to larger (weaker) pressure difference between the two regions, leading to stronger westerlies (easterlies) across the mid-latitudes (Barnston and Livezey, 1987). The two pressure system regions are clearly identified in the stratospheric O_3 response to NAO, particularly in the LSt, with positive regression coefficients above the Labrador–Greenland region and negative coefficients above the Euro-Atlantic region (Fig. 5b). Above these two sectors, the positive phase induces, respectively, an increase and a decrease in LSt O_3 levels. The negative phase is characterized by the opposite behaviour. That NAO pattern is in line with previous studies (Rieder et al., 2013) and was also observed from IASI in tropospheric O_3 (Wespes et al., 2017). The magnitude of annual LSt O_3 changes attributed to NAO variations reaches $\sim$ 20 DU over the in-phase Labrador region (i.e. contribution of 25 % relative to the O_3 variations), while a much lower contribution is found for the MUSt ($\sim$ 4 DU or $\sim$ 10 %). The NAO coeffficient in the LSt also shows that the influence of the NAO extends further into northern Asia in the case of prolonged NAO phases. The NAO has also been shown to influence the propagation of waves into the stratosphere and, hence, the BDC and the strength of the polar vortex in the NH mid-winter (Thompson and Wallace, 2000; Schnadt and Dameris, 2003; Rind et al., 2005). That connection between the NAO and the BDC might explain the negative anomaly in the O_3 response to EPF in the LSt over northern Asia that matches the region of negative response to the NAO.

7. *AAO.* The extratropical circulation of the SH is driven by the Antarctic oscillation that is characterized by geopotential height anomalies south of 20° S, with high anomalies of one sign centered in the polar region and weaker anomalies of the opposing sign north of 55° S (Thompson and Wallace, 2000). This corresponds well to the two band-like regions of opposite signs found for the regression coefficients of adjusted AAO in the LSt (negative coefficients centered in Antarctica and positive coefficient north of $\sim$ 40° S; see Fig. 5b). Similarly to the NAO, the strength of the residual mean circulation and of the polar vortex in the SH are modulated by the AAO through the atmospheric wave activity (Thompson and Wallace, 2000; Thompson and Solomon, 2002). During the positive (negative) phase of the AAO, the BDC is weaker (stronger), leading to less (more) O_3 transported from the tropics into the southern polar region, and the polar vortex is stronger (weaker), leading to more (less) O_3 depletion inside. This likely explains both the positive AAO coefficients in the region north of $\sim$ 40° S (contribution $<\sim$ 5 DU or $\sim$ 10 %) and the negative coefficients around and over the Antarctic (contribution reaching $\sim$ 10 DU or $\sim$ 15 %; exception is found

with positive coefficients over the western Antarctic). The dependence of O_3 variations to the AAO in the MUSt is lower than ~ 7 DU (or ~ 15 %).

8. *ENSO.* Besides the NAO and the AAO, the El Niño–Southern Oscillation is another dominant mode of global climate variability. This coupled ocean-atmosphere phenomenon is governed by sea surface temperature (SST) differences between high tropical and low extratropical Pacific regions (Harrison and Larkin, 1998). Domeisen et al. (2019) have recently reviewed the possible mechanisms connecting the ENSO to the stratosphere in the tropics and the extratropics of both hemispheres. The ozone response to ENSO is represented in Fig. 5 only for the ENSO-lag3 proxy which is found to be the main ENSO proxy contributing to the observed O_3 variations. While in the troposphere, previous works have shown that the ENSO influence mainly results in a high contrast of the regression coefficients between the western Pacific, Indonesian, and northern Australian region and the central and eastern Pacific region caused by reduced rainfall and enhanced O_3 precursor emissions above the western Pacific (called the "chemical effect") (e.g. Oman et al., 2013; Valks et al., 2014; Ziemke et al., 2015; Wespes et al., 2016, and references therein), the LSt O_3 response to ENSO is shown here to translate into a strong tropical–extratropical gradient in the regression coefficients with a negative response in the tropics and a positive response at higher latitudes (~ 5 and ~ 10 DU longitudinal averages, respectively,; see Fig. 6a). In the MUSt, ENSO is globally a smaller out-of-phase driver of O_3 variations (response of ~ 5 DU). The decrease in LSt O_3 during the warm ENSO phase in the tropics (characterized by a negative ENSO lag-3 coefficient reaching 7 DU, or 35 % in the LSt; see Fig. 5) is consistent with the ENSO-modulated upwelling via deep convection in the tropical lower stratosphere and, hence, increased BD circulation (e.g. Randel et al., 2009). The in-phase accumulation of LSt O_3 in the extratropics (contribution reaching 15 DU or 20 %; see Fig. 5) is also consistent with enhanced extratropical planetary waves that propagate into the stratosphere during the warm ENSO phase, resulting in sudden stratospheric warmings and, hence, in enhanced BDC and weaker polar vortices (e.g. Brönnimann et al., 2004; Manzini et al., 2006; Cagnazzo et al., 2009). The very pronounced link between stratospheric O_3 and the ENSO-related dynamical pathways with a time lag of about 3 months is one key finding of the present work. Indeed, the influence of ENSO on stratospheric O_3 measurements has already been reported in earlier studies (Randel and Cobb, 1994; Brönnimann et al., 2004; Randel et al., 2009; Randel and Thompson, 2011; Oman et al., 2013; Manatsa and Mukwada, 2017; Tweedy et al., 2018), but it is the first time that a delayed stratospheric O_3 response is investigated in MLR studies. A 4- to 6-month time lag in O_3 response to ENSO has similarly been identified from IASI in the troposphere (Wespes et al., 2017), where it was explained not only by a tropospheric pathway but also by a specific stratospheric pathway similar to that modulating stratospheric O_3 but with further impact downward onto tropospheric circulation (Butler et al., 2014; Domeisen et al., 2019). Furthermore, the 3-month lag identified in the LSt O_3 response is fully consistent with the modelling work of Cagnazzo et al. (2009), which reports a warming of the polar vortex in February–March following a strong ENSO event (peak activity in November–December) associated with a positive O_3 ENSO anomaly reaching ~ 10 DU in the Arctic and a negative anomaly of ~ 6–7 DU in the Tropics. We find that the tropical–extratropical gradient in O_3 response to ENSO-lag3 is indeed much stronger in spring with contributions of ~ 20–30 DU (see Fig. 7a for the austral spring period vs. winter).

Overall, although the annual MLR model underestimates the O_3 variability at high latitudes ($> 50°$ N–S) by up to 5 DU, particularly in the MUSt (see Fig. 6b), we conclude that it gives a good overall representation of the sources of O_3 variability in the two stratospheric layers sounded by IASI. This is particularly true for the spring period (see Fig. 7) which was studied in several earlier works to reveal the onset of Antarctic total O_3 recovery (Salby et al., 2011; Kuttippurath et al., 2013; Shepherd et al., 2014; Solomon et al., 2016; Weber et al., 2018), despite the large O_3 variability due to the hole formation during that period (~ 80 DU; see Fig. 7a, LSt panel). It is also interesting to see from Fig. 7 that the broad O_3 depletion over Antarctica in the LSt is attributed by the MLR to VPSC (up to 60 DU of explained O_3 variability on a latitudinal average). Following these promising results, below we further analyze the O_3 variability in response to anthropogenic perturbations, assumed in the MLR model by the linear trend term, with a focus over the polar regions.

4 Trend analysis

4.1 10-year trend detection in stratospheric layers

The distributions of the linear trend estimated by the annual regression are represented in Fig. 8a for the MUSt and the LSt (left and right panels, respectively). In agreement with the early signs of O_3 recovery reported for the extratropical middle–upper stratosphere above ~ 25–10 hPa (> 25–30 km; Pawson et al., 2014; Harris et al., 2015; Steinbrecht et al., 2017; Sofieva et al., 2017; Ball et al., 2018), the MUSt shows significant positive trends larger than $1\,\mathrm{DU\,yr^{-1}}$ poleward of $\sim 35°$ N–S (except over Antarctica). The corresponding decadal trends ($> 10\,\mathrm{DU\,decade^{-1}}$) are much larger than the discontinuity of ~ 2–4 DU encountered in the MUSt record

on 15 September 2010 and discussed in Sect. 2.1. The tropical MUSt also shows positive trends but they are weaker ($< 0.8\,\mathrm{DU\,yr^{-1}}$) or not significant. The largest increase is observed in polar O_3 with amplitudes reaching $\sim 2.0\,\mathrm{DU\,yr^{-1}}$. The mid-latitudes also show significant O_3 enhancement, which can be attributed to air mass mixing after the disruption of the polar vortex (Knudsen and Grooss, 2000; Fioletov and Shepherd, 2005; Dhomse et al., 2006; Nair et al., 2015).

As in the MUSt, the LSt is characterized in the southern polar latitudes by significantly positive and large trends (between ~ 1.0 and $2.5\,\mathrm{DU\,yr^{-1}}$). In the mid-latitudes, the lower stratospheric trends are significantly negative, i.e. opposite to those obtained in the MUSt. This highlights the independence between the two O_3 layers sounded by IASI in the stratosphere. Poleward of 25° N the negative LSt trends range between ~ -0.5 and $-1.7\,\mathrm{DU\,yr^{-1}}$. Negative trends in lower stratospheric O_3 have already been reported in extra-polar regions from other space-based measurements (Kyrölä et al., 2013; Gebhardt et al., 2014; Sioris et al., 2014; Harris et al., 2015; Nair et al., 2015; Vigouroux et al., 2015; Wespes et al., 2016; Steinbrecht et al., 2017; Ball et al., 2018) and may be due to changes in stratospheric dynamics at the decadal timescale (Galytska et al., 2019). These previous studies, which were characterized by large uncertainties or resulted from composite-data merging techniques, are confirmed here using a single dataset. The negative trends which are observed at lower stratospheric middle latitudes are difficult to explain with chemistry-climate models (Ball et al., 2018). It is also worth noting that the significant MUSt and LSt O_3 trends are of the same order as those previously estimated from IASI over a shorter period (from 2008 to 2013) and latitudinal averages (see Wespes et al., 2016). This suggests that the trends are not very sensitive to the natural variability in the IASI time series, hence supporting the significance of the O_3 trends presented here.

The sensitivity of IASI O_3 to the estimated trend from MLR is further verified in Fig. 8b, which represents the global distributions of relative differences in the RMSE of the regression residuals obtained with and without a linear trend term included in the MLR model ($(\mathrm{RMSE_{\_w/o\_LT}} - \mathrm{RMSE_{\_with\_LT}})/\mathrm{RMSE_{\_with\_LT}} \times 100$; in percentage). An increase of $\sim 1.0\,\%$–$4.0\,\%$ and $\sim 0.5\,\%$–$2.0\,\%$ in the RMSE is indeed observed for both the MUSt and the LSt, respectively, in regions of significant trend contribution (Fig. 8a), when the trend is excluded. This demonstrates the significance of the trend in improving the performance of the regression. Another statistical method that can be used for evaluating the possibility to infer, from the IASI time period, the significant positive or negative trends in the MUSt and the LSt, respectively, consists of determining the expected year when these specified trends would be detectable from the available measurements (with a probability of 90 %) by taking into account the variance (σ_ε^2) and the autocorrelation (Φ) of the noise residual according to the formalism of Tiao et al. (1990) and Weatherhead et al. (1998). The 95 % confidence interval for that expected trend detection year can also be determined. Such a method has already been used for evaluating the trends derived from IASI in the troposphere (Wespes et al., 2018). It represents a more drastic and conservative method than the standard MLR. The results are displayed in Fig. 8c for an assumed specified trend of $|1.5|\,\mathrm{DU\,yr^{-1}}$, which corresponds to a medium amplitude of trends derived here above from the MLR over the mid-polar regions (Fig. 8a). In the MUSt, we find that $\sim$ 2–3 additional years of IASI measurements would be required to unequivocally detect a trend of $|1.5|\,\mathrm{DU\,yr^{-1}}$ (with probability 0.90) over high latitudes (detectable from ~ 2020–2022 ± 6–12 months), whereas it should already be detectable over the middle and lower latitudes (from $\sim 2015 \pm 3$–6 months). In the LSt, an additional ~ 7 years ($\pm$ 1–2 years) of IASI measurements would be required to categorically identify the probable decline derived from the MLR in northern mid-latitudes, and even more to measure the enhancement in the southern polar latitudes. The longer required measurement period at high latitudes is due to the larger noise residuals in the regression fits (i.e. largest σ_ε) at these latitudes (see Fig. 4a and b). Note that a larger specified trend amplitude would obviously require a shorter period of IASI measurement. We find that only ~ 2 additional years would be required to detect a specified trend of $|2.5|\,\mathrm{DU\,yr^{-1}}$ which characterizes the LSt at high latitudes (data not shown).

4.2 Stratospheric contributions to total O_3 trend

The effect on total O_3 of the counteracting trends in the northern mid-latitudes and of the constructive trends in the southern polar latitudes in the two stratospheric layers sounded by IASI is now investigated.

Figure 9 represents the global distributions of the contribution of the MUSt and the LSt into the total O_3 columns (Fig. 9a; in percentage), of the adjusted trends for the total O_3 (Fig. 9b in $\mathrm{DU\,yr^{-1}}$) and of the estimated year for a $|1.5|\,\mathrm{DU\,yr^{-1}}$ trend detection with a probability of 90 % (Fig. 9c). While no significant change or slightly positive trends in total O_3 after the inflection point in 1997 have been reported on an annual basis (e.g. Weber et al., 2018), Fig. 9b shows clear significant changes: a negative trend at northern mid-latitudes and high latitudes (up to $\sim 2.0\,\mathrm{DU\,yr^{-1}}$ north of 30° N) and positive trend over the southern polar region (up to $\sim 3.0\,\mathrm{DU\,yr^{-1}}$ south of 45° S). Although counteracting trends between lower and upper stratospheric O_3 have been pointed out in the recent study of Ball et al. (2018) to explain the non-significant recovery in total O_3, we find from IASI a dominance of the LSt decline that translates to negative trends over some regions of the NH mid-latitudes and high latitudes in TOC (Fig. 9b). This is explained by the contributions of 45 %–55 % from the LSt to the total column, vs. $\sim 30\,\%$–$40\,\%$ from the MUSt (Fig. 9a) in the mid-latitude and polar regions over the whole year. In addition, the increase in total O_3 at high southern latitudes is dominated

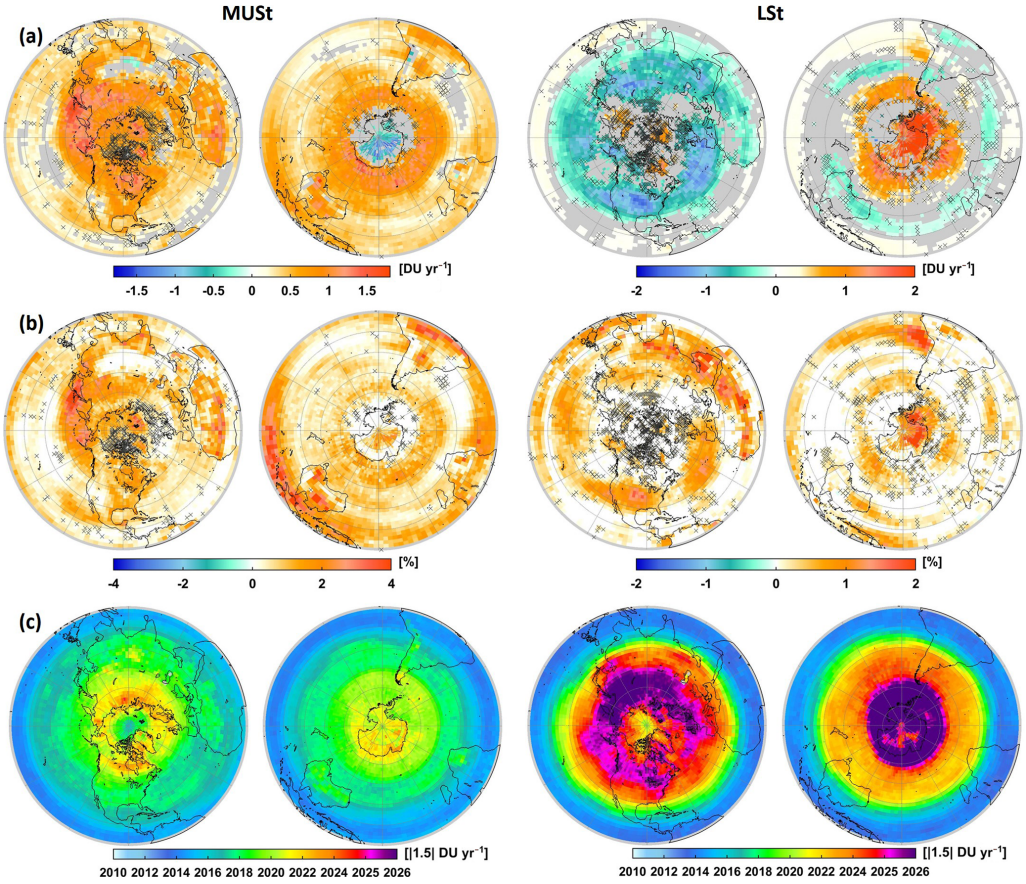

Figure 8. Global distribution **(a)** of the estimated annual trends (in DU yr^{-1}; grey areas and crosses refer to non-significant grid cells within the 95 % confidence limit), **(b)** of the IASI sensitivity to trends calculated as the differences between the RMSE of the annual MLR fits with and without a linear trend term $[(\mathrm{RMSE}_{\mathrm{w/o\_LT}} - \mathrm{RMSE}_{\mathrm{with\_LT}})/\mathrm{RMSE}_{\mathrm{with\_LT}} \times 100]$ (in percentage), **(c)** of the estimated year for a significant detection (with a probability of 90 %) of a given trend of $|1.5|$ DU yr^{-1} starting in January 2008 in MUSt and LSt O_3 columns (left and right panels, respectively). Note that the scales are different for the two layers.

by the LSt, although both layers positively contribute around Antarctica, compared to the trend distributions in Fig. 8. Note that most previous ozone trends studies, including Ball et al. (2018), excluded the polar regions due to limited latitude coverage of some instruments merged in the data composites.

While the annual MLR shows a significant dominance of LSt trends over MUSt trends in the northern mid-latitudes and significant constructive trends in the southern latitudes, total O_3 trends are not ascribed with complete confidence according to the formalism of Tiao et al. (1990) and Weatherhead et al. (1998) discussed in Sect. 4.1. The detectability of a specified trend of $|1.5|$ DU yr^{-1} (Fig. 9c), which corresponds to the medium trend derived from MLR in middle and high latitudes of both hemispheres (Fig. 9b), would need several years of additional measurements to be unequivocal from IASI on an annual basis (from $\sim$ 2022–2024 over the mid-latitudes and from $\sim$ 2035 over the polar regions). A higher trend amplitude of $\sim |2.5|$ DU yr^{-1} derived from the MLR would be observable from $\sim$ 2020–2025 (figure not shown).

The use of the annual MLR could translate to large systematic uncertainties on trends (implying large σ_ε), which induces a longer measurement period required to yield significant trends. These uncertainties could be reduced on a seasonal basis, by attributing different weights to the seasons, which would help in the categorical detection of a specified trend. This is investigated in the subsection below by focusing on the winter and the spring periods.

4.3 Trends in spring and winter

The reports on early signs of total O_3 recovery (Salby et al., 2011; Kuttippurath et al., 2013; Shepherd et al., 2014; Solomon et al., 2016; Kuttippurath and Nair, 2017; Weber et al., 2018) have all focused on the Antarctic region during spring–summer, when the ozone hole area is at its maximum extent, i.e. the LSt O_3 levels at minimum values. Kuttippurath et al. (2018) have, in particular, reported a significant reduction in Antarctic O_3 loss saturation occurrences during spring. Here we investigate the respective contributions of

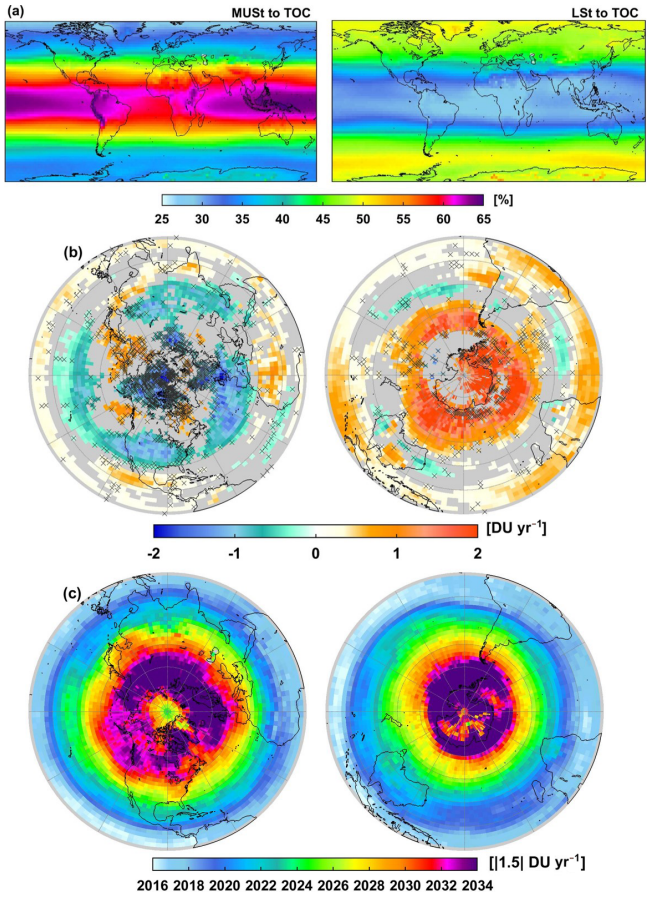

Figure 9. Global distribution of **(a)** the contribution (in percentage) of MUSt and LSt into the total O_3 (left and right panels respectively) averaged over January 2008–December 2017, **(b)** fitted trends in total O_3 (in DU yr^{-1}; the grey areas and crosses refer to the non-significant grid cells in the 95 % confidence limit) and **(c)** estimated year for the detection of a significant trend in total O_3 (with a probability of 90 %) for a given trend of |1.5| DU yr^{-1} starting on January 2008.

the LSt and the MUSt to the TOC recovery over the southern latitudes during spring and also during winter when the minima in O_3 levels occur in the MUSt (down to ~ 60 DU in polar regions), in comparison with the northern latitudes. Figures 10 and 11, respectively, show the SH and the NH distributions of the estimated trends from seasonal MLR (left panels) and of the corresponding year required for a significant detection of |3.0| DU increase per year (right panels) during their respective winter (JJA and DJF; Figs. 10a and 11a) and spring (SON and MAM; Figs. 10b and 11b) for the total, MUSt and LSt O_3 (top, middle and bottom panels, respectively). Figure 10a and b clearly show significant positive trends over Antarctica and the southernmost latitudes of the Atlantic and Indian oceans, with amplitudes ranging between ~ 1 and 5 DU yr^{-1} over latitudes south of ~ 35–40° S in total, MUSt and LSt O_3 ($\sim 3.6 \pm 2.7$, $\sim 3.0 \pm 1.3$, $\sim 3.6 \pm 3.1$ and $\sim 3.7 \pm 1.7$, $\sim 1.3 \pm 0.7$, $\sim 3.7 \pm 1.6$ DU yr^{-1}: spatial averages over JJA and SON for the three O_3 columns, respectively). These trends over 10 years are much larger than the amplitude of the discontinuity in the MUSt time series (Sect. 2.1) and than the trends estimated in Sect. 4.1 (see Fig. 8 for the MUSt and the LSt) and 4.2 (see Fig. 9 for TOC) over the whole year. In MUSt, significant positive trends are observed during each season over the mid-latitudes and polar latitudes of both hemispheres (Figs. 10 and 11 for the winter and spring periods; the other seasons are not shown here) but more particularly in winter and in spring, where the increase reaches a maximum of ~ 4 DU yr^{-1}. In the LSt, the distributions are more complex: the trends are significantly negative in the mid-latitudes of both hemispheres, especially in winter and in spring of the NH, while in spring of the SH, some mid-latitude regions also show near-zero or even positive trends. The southern polar region shows high significant positive trends in winter–spring (see Fig. 10). For the total O_3 at middle to high latitudes, given the mostly counteracting trends detected in the LSt and in the MUSt and the dominance of the LSt over the MUSt (~ 45 %–55 % from the LSt vs. ~ 30 %–40 % from the MUSt into total O_3 over the whole year), these latitudes are governed by negative trends, especially in spring of the NH. High significant increases are detected over polar regions in winter–spring of both hemispheres but more particularly in the SH where the LSt and MUSt trends are both of positive sign.

The substantial winter–spring positive trends observed in MUSt, LSt and total O_3 levels at high latitudes of the SH (and of the NH for the MUSt) are furthermore demonstrated to be detectable from the available IASI measurement period (see Fig. 10, right panels: an assumed increase of |3.0| DU yr^{-1} is detectable from 2016 ± 6 months and from 2018 ± 1 year in the MUSt and the LSt, respectively). The positive trend of ~ 4 DU yr^{-1} measured in polar total O_3 in winter–spring would be observable from $\sim$ 2018–2020 $\pm$ 1–2 years and the decline of ~ -3 DU yr^{-1} in winter–spring of the NH in the LSt would be detectable from $\sim$ 2018–2020 $\pm$9 months (not shown here). Note that the higher negative trends found above the Pacific at the highest latitudes (see Fig. 10) correspond to the regions with longest required measurement period for significant trend detection and, hence, point to poor regression residuals. About ~ 50 % and ~ 35 % of the springtime MUSt and LSt O_3 variations, respectively, are due to anthropogenic factors (estimated by VPSC $\times$ EESC proxy and linear trends in MLR models). This suggests that O_3 changes, especially in the LSt, are mainly governed by dynamics, which contributes to a later projected trend-detection year in comparison with the MUSt (Figs. 10 and 11) and which may hinder the O_3 recovery process.

Overall, the large positive trends estimated concurrently in the LSt, MUSt and total O_3 over the Antarctic region in winter–spring likely reflect the healing of the ozone layer with a decrease in polar ozone depletion (Solomon et al., 2016) and, hence, demonstrate the efficiency of the Montreal Protocol. To the best of our knowledge, these results repre-

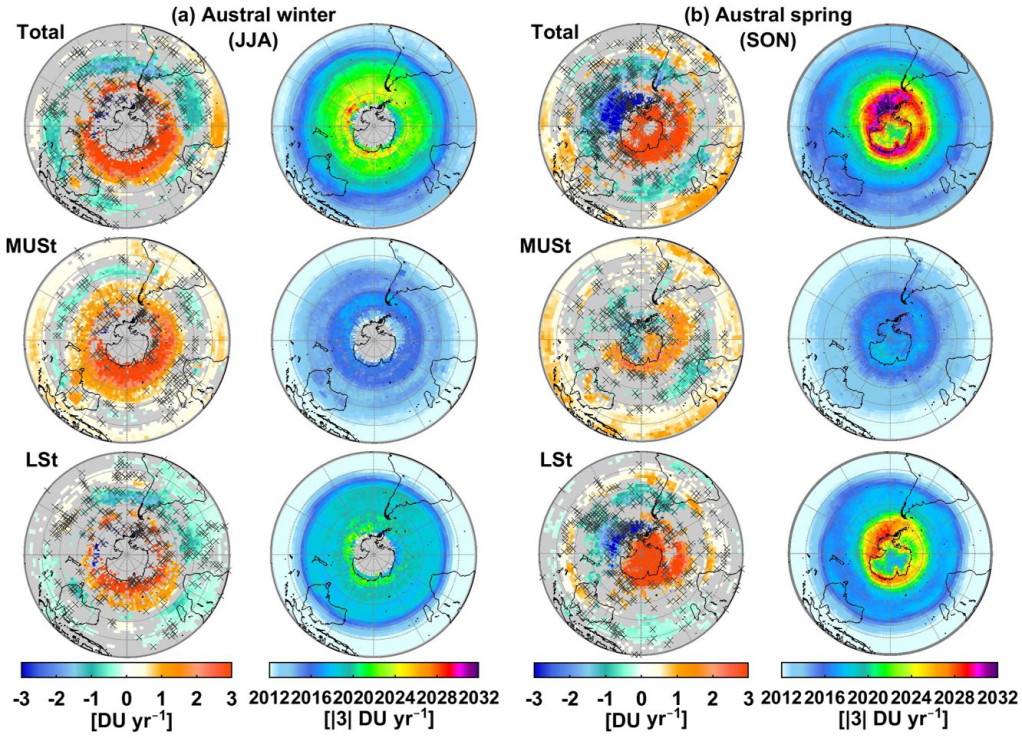

Figure 10. Hemispheric distribution **(a)** in austral winter (JJA) and **(b)** in austral spring (SON) of the estimated trends in total, MUSt and LSt O_3 columns (left panels: top, middle and bottom, respectively; in DU yr^{-1}; the grey areas and crosses refer to the non-significant grid cells within the 95 % confidence limit) and of the corresponding estimated year for a significant trend detection (with a probability of 90 %) of a given trend of |3| DU yr^{-1} starting at January 2008 (right panels: top, middle and bottom, respectively).

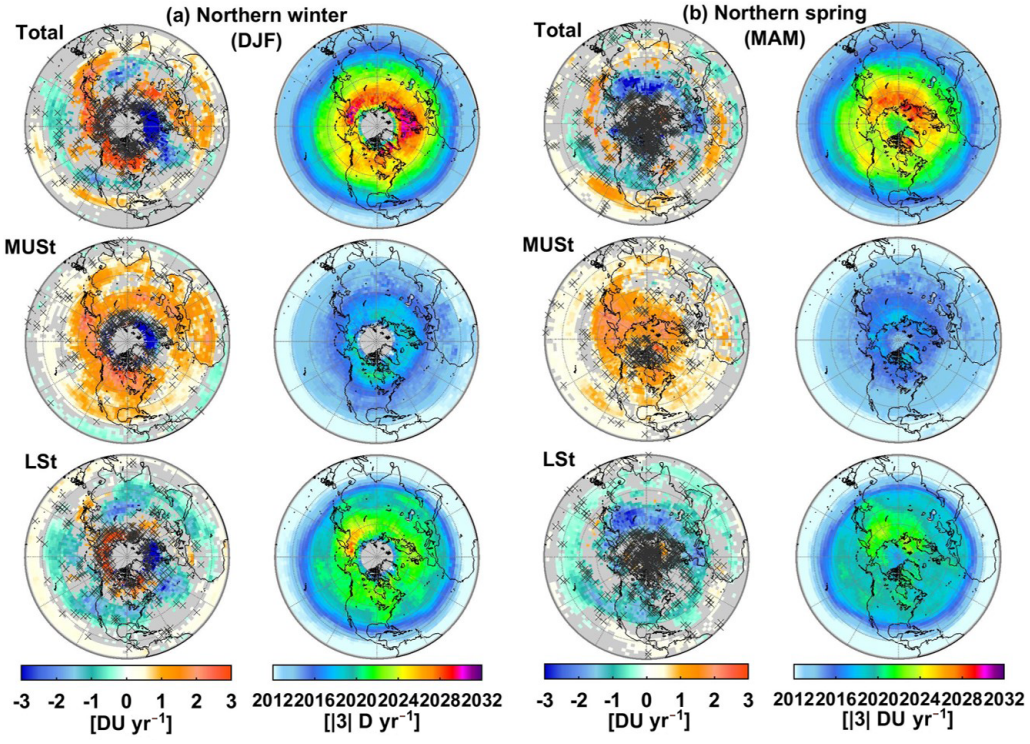

Figure 11. Same as Fig. 10 but **(a)** for the winter (DJF) and **(b)** for the spring (MAM) of the Northern Hemisphere.

sent the first detection of a significant recovery in the stratospheric and the total O_3 columns over the Antarctic from one single satellite dataset.

4.4 Speeding up in O_3 changes

Positive trends in total O_3 over Antarctica were already determined earlier by Solomon et al. (2016) and by Weber et al. (2018) during September over earlier periods ($\sim 2.5\pm1.5\,\mathrm{DU\,yr^{-1}}$ over 2000–2014 and 8.2±6.2 % per decade over 2000–2016, respectively). The larger trends derived from the IASI records (see Fig. 10b; $\sim 3.7\pm1.7\,\mathrm{DU\,yr^{-1}}$ or $\sim 14.4\pm5.8\,\%$ per decade on average in TOC during SON) suggest that the O_3 response could be speeding up due to the accelerating decline of O_3-depleting substances (ODSs) resulting from the Montreal Protocol. This has been investigated here by estimating the change in trend in MUSt, LSt and total O_3 over the IASI mission. Knowing that the length of the measurement period is an important criterion for reducing systematic errors in the trend coefficient determination (i.e. the specific length of natural mode cycles should be covered to avoid any possible compensation effect between the covariates), the ozone response to each natural driver (including VPSC) taken from their adjustment over the whole IASI period (2008–2017; Sect. 3, Fig. 5) is kept fixed. The linear trend term only is adjusted over variable measurement periods that all end in December 2017, by using a single linear iteratively reweighted least squares regression applied on gridded daily IASI time series, after all the sources of natural variability fitted over the full IASI period are removed (typical examples of linear trend adjustment can be found in Fig. S2 of the Supplement). The discontinuity found in the MUSt IASI O_3 records on September 2010 (see Sect. 2.1) is not taken into account in the regression; hence, it might over-represent the trends estimated over periods that start before the jump (i.e. 2008–2017, 2009–2017, 2010–2017). The zonally averaged results are displayed in Fig. 12 for the statistically significant total, MUSt and LSt O_3 trends and their associated uncertainty (accounting for the autocorrelation in the noise residuals; within the 95 % confidence level) estimated from an annual regression. Note that the results are only shown for periods starting before 2015, given that considering shorter periods induces larger standard errors associated with the trends. In the LSt, a clear speeding up in the southern polar O_3 recovery is observed, with amplitudes ranging from $\sim 1.5\pm0.4\,\mathrm{DU\,yr^{-1}}$ over 2008–2017 to $\sim 5.5\pm2.5\,\mathrm{DU\,yr^{-1}}$ over 2015–2017 on zonal averages. Similarly, a speeding up of the O_3 decline at northern mid-latitudes is found with values ranging between $\sim -0.7\pm0.2\,\mathrm{DU\,yr^{-1}}$ over 2008–2017 and $\sim -2.8\pm1.2\,\mathrm{DU\,yr^{-1}}$ over 2015–2017. In the MUSt, a weaker increase is observed over the year around $\sim 60°$ latitude of the SH (from $\sim 0.8\pm0.2\,\mathrm{DU\,yr^{-1}}$ over 2008–2017 to $\sim 2.5\pm1.3\,\mathrm{DU\,yr^{-1}}$ over 2015–2017). Given the positive acceleration in both LSt and MUSt O_3 in the SH, this is where the total O_3 record is characterized by the largest significant recovery (from $\sim 1.7\pm0.7\,\mathrm{DU\,yr^{-1}}$ over 2008–2017 to $\sim 8.0\pm3.5\,\mathrm{DU\,yr^{-1}}$ over 2015–2017). Surprisingly, the speeding up in the O_3 decline in the NH is more pronounced in the total O_3 (from $\sim -1.0\pm0.4\,\mathrm{DU\,yr^{-1}}$ over 2008–2017 to $\sim -5.0\pm2.5\,\mathrm{DU\,yr^{-1}}$ over 2015–2017) compared to the LSt, despite the opposite trend in MUSt O_3. This could reflect the O_3 decline observed in the northern latitudes in the troposphere ($\sim -0.5\,\mathrm{DU\,yr^{-1}}$ over 2008–2016; see Wespes et al., 2018), which is included in the total column.

Overall, the larger annual significant trend amplitudes derived over the last few years of total, MUSt and LSt O_3 measurements, compared with those derived from the whole studied period (Sect. 4.1 and 4.2) and from earlier studies, translate to trends that remain detectable over the increasing uncertainty associated with the shorter and shorter time segments (see Fig. S3 of the Supplement), especially in both LSt and total O_3 in the SH. This demonstrates that we progress towards a significant emergence and speeding up of the O_3 recovery process in the stratosphere over the whole year. Nevertheless, we calculated that additional years of IASI measurements would help in confirming the changes in O_3 recovery and decline over the IASI period (e.g. ~ 4 additional years are required to verify the trends calculated over the 2015–2017 segment in the highest latitudes in the LSt). In addition, a longer measurement period would be useful to derive trends over successive segments of the same length that are long enough to reduce the uncertainty, in order to make the trend and its associated uncertainty more comparable across the fit.

5 Summary and conclusion

In this study, we have analysed the changes in stratospheric O_3 levels sounded by IASI-A by examining the global pictures of natural and anthropogenic sources of O_3 changes independently in the lower (150–25 hPa) and in the middle–upper stratosphere (< 25 hPa). We have exploited to that end a multi-linear regression model that has been specifically developed for the analysis of stratospheric processes by including a series of drivers known to have a causal relationship to natural stratospheric O_3 variations, namely SF, QBO-10, QBO-30, NAO, AAO, ENSO, AERO, EPF and VPSC. We have first verified the representativeness of the O_3 response to each of these natural drivers and found for most of them characteristic patterns that are in line with the current knowledge of their dynamical influence on O_3 variations. One of the most important findings related to the O_3 driver analysis relied on the detection of a very clear time lag of 3 months in the O_3 response to ENSO in the LSt, with a pronounced contrast between an in-phase response in the extratropics and an out-of-phase response in the tropics, which is consistent with the ENSO-modulated dynamic. The 3-month lag observed in the lower stratosphere is also coherent with the 4-to-6-month

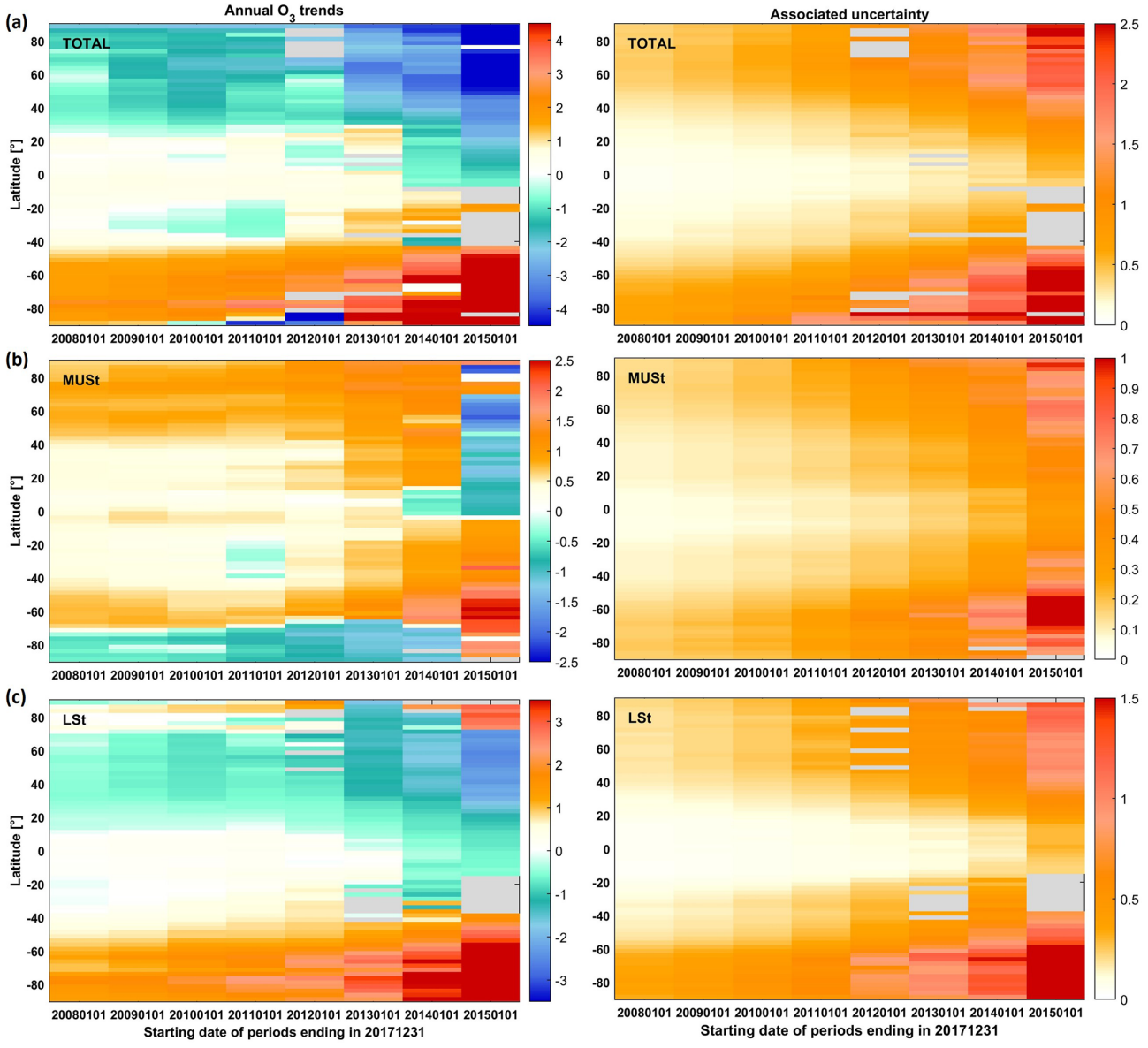

Figure 12. Evolution of estimated linear trend (DU yr^{-1}) and associated uncertainty accounting for the autocorrelation in the noise residuals (DU yr^{-1}; within the 95 % confidence level) in **(a)** total, **(b)** MUSt and **(c)** LSt O_3 columns, as a function of the covered IASI measurement period ending in December 2017, with all natural contributions estimated from the whole IASI period (2008–2017; date format in the figure is yyyyddmm). Note that the scales are different between the columns.

lag detected from a previous study in the troposphere (Wespes et al., 2017) and further supports the stratospheric pathway suggested in Butler et al. (2014) to explain an ENSO influence over a long distance. The representativeness of the influence of the O_3 drivers was also confirmed on a seasonal basis (e.g. high ENSO-lag3 effect in spring, strong VPSC and AERO influences during the austral spring). These results have verified the performance of the regression models (annual and seasonal) to properly discriminate between natural and anthropogenic drivers of O_3 changes. The anthropogenic influence has been evaluated with the linear trend adjustment in the MLR. The main results are summarized as follows.

A highly probable (within 95 %) recovery process is derived from the annual MLR at high southern latitudes in the two stratospheric layers and, therefore, in the total column. It is also derived at high northern latitudes in the MUSt. However, a longer period of IASI measurements is needed to unequivocally demonstrate a positive trend on an annual basis in the IASI record. Only ∼ 2–3 additional years of IASI measurements are required in the MUSt.

A likely O_3 decline (within 95 %) is measured in the lower stratosphere at mid-latitudes, specifically, of the NH, but it would require an additional ~ 7 years of IASI measurements to be categorically confirmed. Given the large contribution from the LSt to the total column (~ 45 %–50 % from LSt vs. ~ 35 % from the MUSt to TOCs), the decline is also calculated in total O_3 with ~ 4–6 years of additional measurements for the trend to be unequivocal.

A significant O_3 recovery is categorically found in the two stratospheric layers ($>\sim 35°$ N–S in the MUSt and $>\sim 45°$ S in the LSt) as well as in the total column ($>\sim 45°$ S) during the winter–spring period, which confirms previous studies that showed healing in the Antarctic O_3 hole with a decrease in its areal extent. These results verify the efficacy of the ban on O_3-depleting substances imposed by the Montreal Protocol and its amendments, throughout the stratosphere and in the total column, from only one single satellite dataset for the first time.

The decline observed in LSt O_3 at northern mid-latitudes is unequivocal over the available IASI measurements in winter–spring of the NH. The exact reasons for that decline are still unknown but O_3 changes in the LSt are estimated to be mainly attributable to dynamics, which likely perturbs the healing of LSt and total O_3 in the NH.

A significant speeding up (within 95 %) in that decline is measured in LSt and total O_3 over the last 10 years (from $\sim -0.7 \pm 0.2\,\mathrm{DU\,yr^{-1}}$ over 2008–2017 to $\sim -2.8 \pm 1.2\,\mathrm{DU\,yr^{-1}}$ over 2015–2017 in LSt O_3 on zonal averages). Even if the acceleration cannot be categorically confirmed yet, it is of particular urgency to understand its causes for apprehending its possible impact on the O_3 layer and on future climate changes.

A clear and significant speeding up (within 95 %) in stratospheric and total O_3 recovery is measured at southern latitudes (e.g. from $\sim 1.5 \pm 0.4\,\mathrm{DU\,yr^{-1}}$ over 2008–2017 to $\sim 5.5 \pm 2.5\,\mathrm{DU\,yr^{-1}}$ over 2015–2017 in the LSt), which translates to trend values that would be categorically detectable in the next few years on an annual basis. It demonstrates that we are currently progressing towards a substantial emergence in O_3 healing in the stratosphere over the whole year in the SH.

Additional years of IASI measurements that will be provided by the in-flight operational IASI-C (2018) and the upcoming IASI-Next Generation (IASI-NG) instrument on board the Metop Second Generation (Metop-SG) series of satellites would be of particular interest to confirm and monitor, in the near future and over a longer period, the speeding up in the O_3 healing of the SH as well as in the LSt O_3 decline measured at mid-latitudes of the NH. IASI-NG/Metop-SG is expected to extend the data record much further in the future (Clerbaux and Crevoisier, 2013; Crevoisier et al., 2014).

Data availability. The IASI O_3 data processed with FORLI-O_3 v0151001 can be downloaded from the Aeris portal at http://iasi.aeris-data.fr/O3/ (last access: 13 September 2019).

Supplement. The supplement related to this article is available online at: https://doi.org/10.5194/acp-19-14031-2019-supplement.

Author contributions. CW performed the analysis, wrote the paper and prepared the figures. DH was responsible for the retrieval algorithm development and the processing of the IASI O_3 dataset. All co-authors contributed to the analysis and reviewed the paper.

Competing interests. The authors declare that they have no conflict of interest.

Acknowledgements. IASI has been developed and built under the responsibility of the Centre National d'Etudes Spatiales (CNES, France). It is flown on board the Metop satellites as part of the EUMETSAT Polar System. The IASI L1 data are received through the EUMETCast near real time data distribution service. We acknowledge the financial support from the ESA O_3-CCI and Copernicus O_3-C3S projects. FORLI-O_3 is being implemented at Eumetsat with the support of the AC SAF project. The research in Belgium is also funded by the Belgian State Federal Office for Scientific, Technical and Cultural Affairs and the European Space Agency (ESA Prodex IASI Flow and B-AC SAF). We acknowledge Ingo Wohltmann (Alfred Wagner Institute, Postdam, Germany) as well as Beiping Luo (Institute for Atmosphere and Climate, ETH Zurich, Switzerland) and Larry Thomason (NASA Langley Research Center, Hampton, USA), for processing and providing datasets of volume of polar stratospheric clouds and of sulfuric acid extinction coefficients, respectively. We are also grateful to Maxime Prignon (Université de Liège, Liège, Belgium) for providing several years of BASCOE simulations.

Review statement. This paper was edited by Jayanarayanan Kuttippurath and reviewed by two anonymous referees.

References

Anderson, J., Russell, J. M., Solomon, S., and Deaver, L. E.: Halogen Occultation Experiment confirmation of stratospheric chlorine decreases in accordance with the Montreal Protocol, J. Geophys. Res.-Atmos., 105, 4483–4490, https://doi.org/10.1029/1999JD901075, 2000.

Baldwin, M. P., Gray, L. J., Dunkerton, T. J., Hamilton, K., Haynes, P. H., Randel, W. J., Holton, J. R., Alexander, M. J., Hirota, I., Horinouchi, T., Jones, D. B. A., Kinnersley, J. S., Marquardt, C., Sato, K., and Takahashi, M.: The quasi-biennial oscillation, Rev. Geophys., 39, 179–230, https://doi.org/10.1029/1999RG000073, 2001.

Ball, W. T., Alsing, J., Mortlock, D. J., Staehelin, J., Haigh, J. D., Peter, T., Tummon, F., Stübi, R., Stenke, A., Anderson, J., Bourassa, A., Davis, S. M., Degenstein, D., Frith, S., Froidevaux, L., Roth, C., Sofieva, V., Wang, R., Wild, J., Yu, P., Ziemke, J. R., and Rozanov, E. V.: Evidence for a continuous decline in lower stratospheric ozone offsetting ozone layer recovery, At-

mos. Chem. Phys., 18, 1379–1394, https://doi.org/10.5194/acp-18-1379-2018, 2018.

Barnston, A. G. and Livezey, R. E.: Classification, seasonality and persistence of low-frequency atmospheric circulation patterns, Mon. Weather Rev., 115, 1083–1126, 1987.

Boynard, A., Hurtmans, D., Garane, K., Goutail, F., Hadji-Lazaro, J., Koukouli, M. E., Wespes, C., Vigouroux, C., Keppens, A., Pommereau, J.-P., Pazmino, A., Balis, D., Loyola, D., Valks, P., Sussmann, R., Smale, D., Coheur, P.-F., and Clerbaux, C.: Validation of the IASI FORLI/EUMETSAT ozone products using satellite (GOME-2), ground-based (Brewer–Dobson, SAOZ, FTIR) and ozonesonde measurements, Atmos. Meas. Tech., 11, 5125–5152, https://doi.org/10.5194/amt-11-5125-2018, 2018.

Brasseur, G.: The response of the middle atmosphere to long-term and short-term solar variability: A two-dimensional model, J. Geophys. Res., 98, 23079–23090, 1993.

Brönnimann, S., Luterbacher, J., Staehelin, J., Svendby, T. M., Hansen, G., and Svenøe, T.: Extreme climate of the global troposphere and stratosphere 1940–1942 related to El Nino, Nature, 431, 971–974, 2004.

Brunner, D., Staehelin, J., Maeder, J. A., Wohltmann, I., and Bodeker, G. E.: Variability and trends in total and vertically resolved stratospheric ozone based on the CATO ozone data set, Atmos. Chem. Phys., 6, 4985–5008, https://doi.org/10.5194/acp-6-4985-2006, 2006.

Buffet, L., Villaret, C., Jacquette, E., Vandermarcq, O., Astruc, P., and Anstötz, S.: Status of IASI instruments onboard Metop-A and Metop-B satellites, 4th IASI International Conference, Antibes Juan-Les-Pins, France, 11–15 April 2016, available at: https://iasi.cnes.fr/sites/default/files/drupal/201612/default/bpc_iasi-conference4-1_02_instruments_buffet.pdf (last access: 30 August 2018), 2016.

Butler, A. H., Polvani, M., and Deser, C.: Separating the stratospheric and tropospheric pathways of El Niño–Southern Oscillation teleconnections, Environ. Res. Lett., 9, 024014, https://doi.org/10.1088/1748-9326/9/2/024014, 2014.

Cagnazzo, C., Manzini, E., Calvo, N., Douglass, A., Akiyoshi, H., Bekki, S., Chipperfield, M., Dameris, M., Deushi, M., Fischer, A. M., Garny, H., Gettelman, A., Giorgetta, M. A., Plummer, D., Rozanov, E., Shepherd, T. G., Shibata, K., Stenke, A., Struthers, H., and Tian, W.: Northern winter stratospheric temperature and ozone responses to ENSO inferred from an ensemble of Chemistry Climate Models, Atmos. Chem. Phys., 9, 8935–8948, https://doi.org/10.5194/acp-9-8935-2009, 2009.

Chabrillat, S., Vigouroux, C., Christophe, Y., Engel, A., Errera, Q., Minganti, D., Monge-Sanz, B. M., Segers, A., and Mahieu, E.: Comparison of mean age of air in five reanalyses using the BASCOE transport model, Atmos. Chem. Phys., 18, 14715–14735, https://doi.org/10.5194/acp-18-14715-2018, 2018.

Chipperfield, M. P., Kinnersley, J. S., and Zawodny, J.: A twodimensional model study of the QBO signal in SAGE II NO_2 and O_3, Geophys. Res. Lett., 21, 589–592, 1994.

Chubachi, S.: Preliminary results of ozone observations at Syowa Station from February 1982 to January 1983, in: Proc. Sixth Symposium on Polar Meteorology and Glaciology, edited by: Kusunoki, K., Vol. 34 of Mem. National Institute of Polar Research Special Issue, 13–19, 1984.

Clarisse, L., Clerbaux, C., Franco, B., Hadji-Lazaro, J., Whitburn, S., Kopp, A. K., Hurtmans, D., and Coheur, P.-F.: A decadal data set of global atmospheric dust retrieved from IASI satellite measurements, J. Geophys. Res., 124, 1618–1647, https://doi.org/10.1029/2018JD029701, 2019.

Coldewey-Egbers, M., Loyola R., D. G., Braesicke, P., Dameris, M., van Roozendael, M., Lerot, C., and Zimmer, W.: A new health check of the ozone layer at global and regional scales, Geophys. Res. Lett., 41, 4363–4372, https://doi.org/10.1002/2014GL060212, 2014.

Clerbaux, C. and Crevoisier, C.: New Directions: Infrared remote sensing of the troposphere from satellite: Less, but better, Atmos. Environ., 72, 24–26, 2013.

Clerbaux, C., Boynard, A., Clarisse, L., George, M., Hadji-Lazaro, J., Herbin, H., Hurtmans, D., Pommier, M., Razavi, A., Turquety, S., Wespes, C., and Coheur, P.-F.: Monitoring of atmospheric composition using the thermal infrared IASI/MetOp sounder, Atmos. Chem. Phys., 9, 6041–6054, https://doi.org/10.5194/acp-9-6041-2009, 2009.

Crevoisier, C., Clerbaux, C., Guidard, V., Phulpin, T., Armante, R., Barret, B., Camy-Peyret, C., Chaboureau, J.-P., Coheur, P.-F., Crépeau, L., Dufour, G., Labonnote, L., Lavanant, L., Hadji-Lazaro, J., Herbin, H., Jacquinet-Husson, N., Payan, S., Péquignot, E., Pierangelo, C., Sellitto, P., and Stubenrauch, C.: Towards IASI-New Generation (IASI-NG): impact of improved spectral resolution and radiometric noise on the retrieval of thermodynamic, chemistry and climate variables, Atmos. Meas. Tech., 7, 4367–4385, https://doi.org/10.5194/amt-7-4367-2014, 2014.

Crutzen, P. J.: Estimates of possible future ozone reductions from continued use of fluoro-chloro-methanes (CF2Cl2, CFCl3), Geophys. Res. Lett., 1, 205–208, https://doi.org/10.1029/GL001i005p00205, 1974.

Dhomse, S., Weber, M., Wohltmann, I., Rex, M., and Burrows, J. P.: On the possible causes of recent increases in northern hemispheric total ozone from a statistical analysis of satellite data from 1979 to 2003, Atmos. Chem. Phys., 6, 1165–1180, https://doi.org/10.5194/acp-6-1165-2006, 2006.

Dhomse, S. S., Chipperfield, P., Feng, W., Hossaini, R., Mann G. W., and Santee, M. L.: Revisiting the hemispheric asymmetry in midlatitude ozone changes following the Mount Pinatubo eruption: A 3-D model study, Geophys. Res. Lett., 42, 3038–3047, 2015.

Domeisen, D. I., Garfinkel, C. I., and Butler, A. H.: The teleconnection of El Niño Southern Oscillation to the stratosphere, Rev. Geophys., 57, 5–47, https://doi.org/10.1029/2018RG000596, 2019.

Errera, Q., Chabrillat, S., Christophe, Y., Debosscher, J., Hubert, D., Lahoz, W., Santee, M. L., Shiotani, M., Skachko, S., von Clarmann, T., and Walker, K.: Technical note: Reanalysis of Aura MLS Chemical Observations, Atmos. Chem. Phys. Discuss., https://doi.org/10.5194/acp-2019-530, in review, 2019.

Farman, J. C., Gardiner, B. G., and Shanklin, J. D.: Large losses of total ozone in Antarctica reveal seasonal ClO_x/NO_x interaction, Nature, 315, 207–210, https://doi.org/10.1038/315207a0, 1985.

Farmer, C. B., Toon, G. C., Shaper, P. W., Blavier, J. F., and Lowes, L. L.: Stratospheric trace gases in the spring 1986 Antarctic atmosphere, Nature, 329, 126–130, 1987.

Fioletov, V. E. and Shepherd, T. G.: Seasonal persistence of midlatitude total ozone anomalies, Geophys. Res. Lett., 30, 1417, https://doi.org/10.1029/2002GL016739, 2003.

Fioletov, V. E. and Shepherd, T. G.: Summertime total ozone variations over middle and polar latitudes, Geophys. Res. Lett, 32, 4807, https://doi.org/10.1029/2004GL022080, 2005.

Frossard, L., Rieder, H. E., Ribatet, M., Staehelin, J., Maeder, J. A., Di Rocco, S., Davison, A. C., and Peter, T.: On the relationship between total ozone and atmospheric dynamics and chemistry at mid-latitudes – Part 1: Statistical models and spatial fingerprints of atmospheric dynamics and chemistry, Atmos. Chem. Phys., 13, 147–164, https://doi.org/10.5194/acp-13-147-2013, 2013.

Fusco, A. C. and Salby, M. L.: Interannual variations of total ozone and their relationship to variations of planetary wave activity, J. Climate, 12, 1619–1629, 1999.

Galytska, E., Rozanov, A., Chipperfield, M. P., Dhomse, Sandip. S., Weber, M., Arosio, C., Feng, W., and Burrows, J. P.: Dynamically controlled ozone decline in the tropical mid-stratosphere observed by SCIAMACHY, Atmos. Chem. Phys., 19, 767–783, https://doi.org/10.5194/acp-19-767-2019, 2019.

Gebhardt, C., Rozanov, A., Hommel, R., Weber, M., Bovensmann, H., Burrows, J. P., Degenstein, D., Froidevaux, L., and Thompson, A. M.: Stratospheric ozone trends and variability as seen by SCIAMACHY from 2002 to 2012, Atmos. Chem. Phys., 14, 831–846, https://doi.org/10.5194/acp-14-831-2014, 2014.

Harris, N. R. P., Hassler, B., Tummon, F., Bodeker, G. E., Hubert, D., Petropavlovskikh, I., Steinbrecht, W., Anderson, J., Bhartia, P. K., Boone, C. D., Bourassa, A., Davis, S. M., Degenstein, D., Delcloo, A., Frith, S. M., Froidevaux, L., Godin-Beekmann, S., Jones, N., Kurylo, M. J., Kyrölä, E., Laine, M., Leblanc, S. T., Lambert, J.-C., Liley, B., Mahieu, E., Maycock, A., de Mazière, M., Parrish, A., Querel, R., Rosenlof, K. H., Roth, C., Sioris, C., Staehelin, J., Stolarski, R. S., Stübi, R., Tamminen, J., Vigouroux, C., Walker, K. A., Wang, H. J., Wild, J., and Zawodny, J. M.: Past changes in the vertical distribution of ozone – Part 3: Analysis and interpretation of trends, Atmos. Chem. Phys., 15, 9965–9982, https://doi.org/10.5194/acp-15-9965-2015, 2015.

Harrison, D. E. and Larkin, N. K.: El Niño-Southern Oscillation sea surface temperature and wind anomalies, 1946–1993, Rev. Geophys., 36, 353–399, https://doi.org/10.1029/98RG00715, 1998.

Hilton, F., Armante, R., August, T., Barnet, C., Bouchard, A., Camy-Peyret, C., Capelle, V., Clarisse, L., Clerbaux, C., Coheur, P., Collard, A., Crevoisier, C., Dufour, G., Edwards, D., Faijan, F., Fourrié, N., Gambacorta, A., Goldberg, M., Guidard, V., Hurtmans, D., Illingworth, S., Jacquinet-Husson, N., Kerzenmacher, T., Klaes, D., Lavanant, L., Masiello, G., Matricardi, M., McNally, A., Newman, S., Pavelin, E., Payan, S., Péquignot, E., Peyridieu, S., Phulpin, T., Remedios, J., Schlüssel, P., Serio, C., Strow, L., Stubenrauch, C., Taylor, J., Tobin, D., Wolf, W., and Zhou, D.: Hyperspectral Earth Observation from IASI: Five Years of Accomplishments, B. Am. Meteorol. Soc., 93, 347–370, https://doi.org/10.1175/BAMS-D-11-00027.1, 2012.

Hofmann, D. J. and Oltmans, S. J.: Antarctic ozone during 1992: Evidence for Pinatubo volcanic aerosol effects, J. Geophys. Res., 98, 18555–18561, https://doi.org/10.1029/93JD02092, 1993.

Hofmann, D. J. and Solomon, S.: Ozone destruction through heterogeneous chemistry following the eruption of El Chichón, J. Geophys. Res., 94, 5029, https://doi.org/10.1029/JD094iD04p05029, 1989.

Hofmann, D. J., Oltmans, S. J., Harris, J. M., Johnson, B. J., and Lathrop, J. A.: Ten years of ozonesonde measurements at the south pole: Implications for recovery of springtime Antarctic ozone, J. Geophys. Res., 102, 8931–8943, https://doi.org/10.1029/96JD03749, 1997.

Hood, L. L. and Soukharev, B. E.: Quasi-decadal variability of the tropical lower stratosphere: The role of extratropical wave forcing, J. Atmos. Sci., 60, 2389–2403, 2003.

Hood, L. L. and Soukharev, B. E.: Solar induced variations of odd nitrogen: Multiple regression analysis of UARS HALOE data, Geophys. Res. Lett., 33, L22805, https://doi.org/10.1029/2006GL028122, 2006.

Hood, L. L., McCormick, J. P., and Labitzke, K.: An investigation of dynamical contributions to midlatitude ozone trends in winter, J. Geophys. Res., 102, 13079–13093, 1997.

Hubert, D., Lambert, J.-C., Verhoelst, T., Granville, J., Keppens, A., Baray, J.-L., Bourassa, A. E., Cortesi, U., Degenstein, D. A., Froidevaux, L., Godin-Beekmann, S., Hoppel, K. W., Johnson, B. J., Kyrölä, E., Leblanc, T., Lichtenberg, G., Marchand, M., McElroy, C. T., Murtagh, D., Nakane, H., Portafaix, T., Querel, R., Russell III, J. M., Salvador, J., Smit, H. G. J., Stebel, K., Steinbrecht, W., Strawbridge, K. B., Stübi, R., Swart, D. P. J., Taha, G., Tarasick, D. W., Thompson, A. M., Urban, J., van Gijsel, J. A. E., Van Malderen, R., von der Gathen, P., Walker, K. A., Wolfram, E., and Zawodny, J. M.: Ground-based assessment of the bias and long-term stability of 14 limb and occultation ozone profile data records, Atmos. Meas. Tech., 9, 2497–2534, https://doi.org/10.5194/amt-9-2497-2016, 2016.

Hurrell, J. W.: Decadal trends in the North Atlantic Oscillation regional temperatures and precipitation, Science, 269, 676–679, 1995.

Hurtmans, D., Coheur, P., Wespes, C., Clarisse, L., Scharf, O., Clerbaux, C., Hadji-Lazaro, J., George, M., and Turquety, S.: FORLI radiative transfer and retrieval code for IASI, J. Quant. Spectrosc. Ra., 113, 1391–1408, 2012.

Jackman, C., Fleming, E., and Vitt, F.: Influence of extremely large solar proton events in a changing stratosphere, J. Geophys. Res., 105, 11659–11670, 2000.

Jonsson, A. I., de Grandpré, J., Fomichev, V. I., McConnell, J. C., and Beagley, S. R.: Doubled CO_2-induced cooling in the middle atmosphere: photochemical analysis of the ozone radiative feedback, J. Geophys. Res., 109, D24103, https://doi.org/10.1029/2004JD005093, 2004.

Kalnay, E., Kanamitsu, M., Kistler, R., Collins, W., Deaven, D., Gandin, L., Iredell, M., Saha, S., White, G., Woollen, J., Zhu, Y., Chelliah, M., Ebisuzaki, W., Higgins, W., Janowiak, J., Mo, K. C., Ropelewski, C., Wang, J., Leetmaa, A., Reynolds, R., Jenne, R., and Joseph, D.: The NCEP/NCAR 40-Year Reanalysis Project, B. Am. Meteorol. Soc., 77, 437–472, 1996.

Keeble, J., Brown, H., Abraham, N. L., Harris, N. R. P., and Pyle, J. A.: On ozone trend detection: using coupled chemistry–climate simulations to investigate early signs of total column ozone recovery, Atmos. Chem. Phys., 18, 7625–7637, https://doi.org/10.5194/acp-18-7625-2018, 2018.

Keppens, A., Lambert, J.-C., Granville, J., Hubert, D., Verhoelst, T., Compernolle, S., Latter, B., Kerridge, B., Siddans, R., Boynard, A., Hadji-Lazaro, J., Clerbaux, C., Wespes, C., Hurtmans, D. R., Coheur, P.-F., van Peet, J. C. A., van der A, R. J., Garane, K., Koukouli, M. E., Balis, D. S., Delcloo, A., Kivi, R., Stübi, R., Godin-Beekmann, S., Van Roozendael, M., and Zehner, C.: Quality assessment of the Ozone_cci Climate Research Data

Package (release 2017) – Part 2: Ground-based validation of nadir ozone profile data products, Atmos. Meas. Tech., 11, 3769–3800, https://doi.org/10.5194/amt-11-3769-2018, 2018.

Knudsen, B. M. and Grooss, J.: Northern midlatitude stratospheric ozone dilution in spring modeled with simulated mixing, J. Geophys. Res., 105, 6885–6890, 2000.

Kodera, K. and Kuroda, Y.: Dynamical response to the solar cycle: Winter stratopause and lower stratosphere, J. Geophys. Res., 107, 4749, https://doi.org/10.1029/2002JD002224, 2002.

Kuttippurath, J. and Nair, P. J.: The signs of Antarctic ozone hole recovery 2017, Sci. Rep.-UK, 7, 585, https://doi.org/10.1038/s41598-017-00722-7, 2017.

Kuttippurath, J., Lefèvre, F., Pommereau, J.-P., Roscoe, H. K., Goutail, F., Pazmiño, A., and Shanklin, J. D.: Antarctic ozone loss in 1979–2010: first sign of ozone recovery, Atmos. Chem. Phys., 13, 1625–1635, https://doi.org/10.5194/acp-13-1625-2013, 2013.

Kuttippurath, J., Kumar, P., Nair, P. J., and Pandey, P. C.: Emergence of ozone recovery evidenced by reduction in the occurrence of Antarctic ozone loss saturation, Climate and Atmospheric Science, 1, 2397–3722, https://doi.org/10.1038/s41612-018-0052-6, 2018.

Kyrölä, E., Laine, M., Sofieva, V., Tamminen, J., Päivärinta, S.-M., Tukiainen, S., Zawodny, J., and Thomason, L.: Combined SAGE II–GOMOS ozone profile data set for 1984–2011 and trend analysis of the vertical distribution of ozone, Atmos. Chem. Phys., 13, 10645–10658, https://doi.org/10.5194/acp-13-10645-2013, 2013.

Labitzke, K. and van Loon, H.: The QBO effect on the solar signal in the global stratosphere in the winter of the Northern Hemisphere, J. Atmos. Sol.-Terr. Phy., 62, 621–628, 2000.

Mäder, J. A., Staehelin, J., Brunner, D., Stahel, W. A., Wohltmann, I., and Peter, T.: Statistical modelling of total ozone: Selection of appropriate explanatory variables, J. Geophys. Res., 112, D11108, https://doi.org/10.1029/2006JD007694, 2007.

Mäder, J. A., Staehelin, J., Peter, T., Brunner, D., Rieder, H. E., and Stahel, W. A.: Evidence for the effectiveness of the Montreal Protocol to protect the ozone layer, Atmos. Chem. Phys., 10, 12161–12171, https://doi.org/10.5194/acp-10-12161-2010, 2010.

Manatsa, D. and Mukwada, G.: A connection from stratospheric ozone to El Niño-Southern Oscillation, Sci. Rep.-UK, 7, 5558, https://doi.org/10.1038/s41598-017-05111-8, 2017.

Manzini, E., Giorgetta, M. A., Esch, M., Kornblueh, L., and Roeckner, E.: The influence of sea surface temperatures on the northern winter stratosphere: Ensemble simulations with the MAECHAM5 model, J. Climate, 19, 3863–3881, 2006.

McCormack, J. P., Siskind, D. E., and Hood, L. L.: Solar-QBO interaction and its impact on stratospheric ozone in a zonally averaged photochemical transport model of the middle atmosphere, J. Geophys. Res., 112, D16109, https://doi.org/10.1029/2006JD008369, 2007.

McPeters, R. D., Labow, G. J., and Logan, J. A.: Ozone climatological profiles for satellite retrieval algorithms, J. Geophys. Res.-Atmos., 112, D05308, https://doi.org/10.1029/2005JD006823, 2007.

Molina, M. J. and Rowland, F. S.: Stratospheric sink for chlorofluoromethanes: Chlorine atom-catalysed destruction of ozone, Nature, 249, 810–812, 1974.

Nair, P. J., Froidevaux, L., Kuttippurath, J., Zawodny, J. M., Russell, J. M., Steinbrecht, W., Claude, H., Leblanc, T., van Gijsel, J. A. E., Johnson, B., Swart, D. P. J., Thomas, A., Querel, R., Wang, R., and Anderson, J.: Subtropical and midlatitude ozone trends in the stratosphere: Implications for recovery, J. Geophys. Res.-Atmos., 120, 7247–7257, https://doi.org/10.1002/2014JD022371, 2015.

Newchurch, M. J., Yang, E.-S., Cunnold, D. M., Reinsel, G. C., Zawodny, J. M., and Russell III, J. M.: Evidence for slowdown in stratospheric ozone loss: First stage of ozone recovery, J. Geophys. Res., 108, 4507, https://doi.org/10.1029/2003JD003471, 2003.

Newman, P. A., Nash, E. R., Kawa, S. R., Montzka, S. A., and Schauffler, S. M.: When will the Antarctic ozone hole recover?, Geophys. Res. Lett., 33, L12814, https://doi.org/10.1029/2005GL025232, 2006.

Oman, L. D., Douglass, A. R., Ziemke, J. R., Rodriguez, J. M., Waugh, D. W., and Nielsen, J. E.: The ozone response to ENSO in Aura satellite measurements and a chemistry–climate simulation, J. Geophys. Res.-Atmos., 118, 965–976, 2013.

Pawson, S., Steinbrecht, W., Charlton-Perez, A. J., Fujiwara, M., Karpechko, A. Y., Petropavlovskikh, I., Urban, J., and Weber, M.: Update on Global Ozone: Past, Present, and Future, in: Scientific Assessment of Ozone Depletion: 2014, World Meteorological Organization, Global Ozone Research and Monitoring Project – Report No. 55, chap. 2, World Meteorological Organization/UNEP, Geneva, Switzerland, 2014.

Portmann, R. W., Solomon, S., Garcia, R. R., Thomason, L. W., Poole, L. R., and McCormick, M. P.: Role of aerosol variations in anthropogenic ozone depletion in the polar regions, J. Geophys. Res., 101, 22991–23006, https://doi.org/10.1029/96JD02608, 1996.

Randel, W. J. and Cobb, J. B.: Coherent variations of monthly mean total ozone and lower stratospheric temperature, J. Geophys. Res.-Atmos., 99, 5433–5447, 1994.

Randel, W. J. and Thompson, A. M.: Interannual variability and trends in tropical ozone derived from SAGE II satellite data and SHADOZ ozonesondes, J. Geophys. Res., 116, D07303, https://doi.org/10.1029/2010JD015195, 2011.

Randel, W. J. and Wu, F.: Isolation of the ozone QBO in SAGE II data by singular-value decomposition, J. Atmos. Sci., 53, 2546–2559, 1996.

Randel, W. J., Wu, F., and Stolarski, R.: Changes in column ozone correlated with the stratospheric EP flux, J. Meteorol. Soc. Jpn., 80, 849–862, 2002.

Randel, W. J., Garcia, R. R., Calvo, N., and Marsh, D.: ENSO influence on zonal mean temperature and ozone in the tropical lower stratosphere, Geophys. Res. Lett., 36, L15822, https://doi.org/10.1029/2009GL039343, 2009.

Reinsel, G. C., Miller, A. J., Weatherhead, E. C., Flynn, L. E., Nagatani, R. M., Tiao, G. C., and Wuebbles, D. J.: Trend analysis of total ozone data for turnaround and dynamical contributions, J. Geophys. Res., 110, D16306, https://doi.org/10.1029/2004JD004662, 2005.

Revell, L. E., Stenke, A., Luo, B., Kremser, S., Rozanov, E., Sukhodolov, T., and Peter, T.: Impacts of Mt Pinatubo volcanic aerosol on the tropical stratosphere in chemistry–climate model simulations using CCMI and CMIP6 strato-

spheric aerosol data, Atmos. Chem. Phys., 17, 13139–13150, https://doi.org/10.5194/acp-17-13139-2017, 2017.

Rex, M., Salawitch, R. J., von der Gathen, P., Harris, N. R. P., Chipperfield, M. P., and Naujokat, B.: Arctic ozone loss and climate change, Geophys. Res. Lett., 32, L04116, https://doi.org/10.1029/2003GL018844, 2004.

Rieder, H. E., Frossard, L., Ribatet, M., Staehelin, J., Maeder, J. A., Di Rocco, S., Davison, A. C., Peter, T., Weihs, P., and Holawe, F.: On the relationship between total ozone and atmospheric dynamics and chemistry at mid-latitudes – Part 2: The effects of the El Niño/Southern Oscillation, volcanic eruptions and contributions of atmospheric dynamics and chemistry to long-term total ozone changes, Atmos. Chem. Phys., 13, 165–179, https://doi.org/10.5194/acp-13-165-2013, 2013.

Rind, D., Perlwitz, J., and Lonergan, P.: AO/NAO response to climate change: 1. Respective influences of stratospheric and tropospheric climate changes, J. Geophys. Res., 110, D12107, https://doi.org/10.1029/2004JD005103, 2005.

Rodgers, C. D.: Inverse Methods for Atmospheric Sounding: Theory and Practice, World Scientific, Series on Atmospheric, Oceanic and Planetary Physics, 2, Hackensack, N.J., 2000.

Roscoe, H. K. and Haigh, J. D.: Influences of ozone depletion, the solar cycle and the QBO on the Southern Annular Mode, Q. J. Roy. Meteor. Soc., 133, 1855–1864, 2007.

Salby, M., Titova, E., and Deschamps, L.: Rebound of Antarctic ozone, Geophys. Res. Lett., 38, L09702, https://doi.org/10.1029/2011GL047266, 2011.

Schnadt, C. and Dameris, M.: Relationship between North Atlantic Oscillation changes and stratospheric ozone recovery in the Northern Hemisphere in a chemistry-climate model, J. Geophys. Res., 30, 1487, https://doi.org/10.1029/2003GL017006, 2003.

Shepherd, T. G., Plummer, D. A., Scinocca, J. F., Hegglin, M. I., Fioletov, V. E., Reader, M. C., Remsberg, E., von Clarmann, T., and Wang, H. J.: Reconciliation of halogen-induced ozone loss with the total-column ozone record, Nat. Geosci., 7, 443–449, https://doi.org/10.1038/ngeo2155, 2014.

Sioris, C. E., McLinden, C. A., Fioletov, V. E., Adams, C., Zawodny, J. M., Bourassa, A. E., Roth, C. Z., and Degenstein, D. A.: Trend and variability in ozone in the tropical lower stratosphere over 2.5 solar cycles observed by SAGE II and OSIRIS, Atmos. Chem. Phys., 14, 3479–3496, https://doi.org/10.5194/acp-14-3479-2014, 2014.

Sofieva, V. F., Kyrölä, E., Laine, M., Tamminen, J., Degenstein, D., Bourassa, A., Roth, C., Zawada, D., Weber, M., Rozanov, A., Rahpoe, N., Stiller, G., Laeng, A., von Clarmann, T., Walker, K. A., Sheese, P., Hubert, D., van Roozendael, M., Zehner, C., Damadeo, R., Zawodny, J., Kramarova, N., and Bhartia, P. K.: Merged SAGE II, Ozone_cci and OMPS ozone profile dataset and evaluation of ozone trends in the stratosphere, Atmos. Chem. Phys., 17, 12533–12552, https://doi.org/10.5194/acp-17-12533-2017, 2017.

Solomon, P., Barrett, J., Mooney, T., Connor, B., Parrish, A., and Siskind, D. E.: Rise and decline of active chlorine in the stratosphere, Geophys. Res. Lett., 33, L18807, https://doi.org/10.1029/2006GL027029, 2006.

Solomon, S.: Stratospheric ozone depletion: A review of concepts and history, Rev. Geophys., 37, 275–316, https://doi.org/10.1029/1999RG900008, 1999.

Solomon, S., Garcia, R. R., Rowland, F. S., and Wuebbles, D. J.: On the depletion of Antarctic zone, Nature, 321, 755–758, 1986.

Solomon, S., Portman, R. W., Garcia, R. R., Thomason, L. W., Poole, L. R., and McCormack, M. P.: The role of aerosol variations in anthropogenic ozone depletion at northern midlatitudes, J. Geophys. Res., 101, 6713–6727, 1996.

Solomon, S., Ivy, D. J., Kinnison, D., Mills, M. J., Neely, R. R., and Schmidt, A.: Emergence of healing in the Antarctic ozone layer, Science, 353, 269–274, https://doi.org/10.1126/science.aae0061, 2016.

Soukharev, B. E. and Hood, L. L.: Solar cycle variation of stratospheric ozone: Multiple regression analysis of long-term satellite data sets and comparisons with models, J. Geophys. Res., 111, D20314, https://doi.org/10.1029/2006JD007107, 2006.

Stolarski, R. S., Krueger, A. J., Schoeberl, M. R., Mc-Peters, R. D., Newman, P. A., and Alpert, J. C.: Nimbus 7 satellite measurements of the springtime Antarctic ozone decrease, Nature, 322, 808–811, 1986.

Steinbrecht, W., Hassler, B., Claude, H., Winkler, P., and Stolarski, R. S.: Global distribution of total ozone and lower stratospheric temperature variations, Atmos. Chem. Phys., 3, 1421–1438, https://doi.org/10.5194/acp-3-1421-2003, 2003.

Steinbrecht, W., Haßler, B., Brühl, C., Dameris, M., Giorgetta, M. A., Grewe, V., Manzini, E., Matthes, S., Schnadt, C., Steil, B., and Winkler, P.: Interannual variation patterns of total ozone and lower stratospheric temperature in observations and model simulations, Atmos. Chem. Phys., 6, 349–374, https://doi.org/10.5194/acp-6-349-2006, 2006.

Steinbrecht, W., Froidevaux, L., Fuller, R., Wang, R., Anderson, J., Roth, C., Bourassa, A., Degenstein, D., Damadeo, R., Zawodny, J., Frith, S., McPeters, R., Bhartia, P., Wild, J., Long, C., Davis, S., Rosenlof, K., Sofieva, V., Walker, K., Rahpoe, N., Rozanov, A., Weber, M., Laeng, A., von Clarmann, T., Stiller, G., Kramarova, N., Godin-Beekmann, S., Leblanc, T., Querel, R., Swart, D., Boyd, I., Hocke, K., Kämpfer, N., Maillard Barras, E., Moreira, L., Nedoluha, G., Vigouroux, C., Blumenstock, T., Schneider, M., García, O., Jones, N., Mahieu, E., Smale, D., Kotkamp, M., Robinson, J., Petropavlovskikh, I., Harris, N., Hassler, B., Hubert, D., and Tummon, F.: An update on ozone profile trends for the period 2000 to 2016, Atmos. Chem. Phys., 17, 10675–10690, https://doi.org/10.5194/acp-17-10675-2017, 2017.

Thomason, L. W., Ernest, N., Millán, L., Rieger, L., Bourassa, A., Vernier, J.-P., Manney, G., Luo, B., Arfeuille, F., and Peter, T.: A global space-based stratospheric aerosol climatology: 1979–2016, Earth Syst. Sci. Data, 10, 469–492, https://doi.org/10.5194/essd-10-469-2018, 2018.

Thompson, D. W. J. and Solomon, S.: Interpretation of Recent Southern Hemisphere Climate Change, Science, 296, 895–899, 2002.

Thompson, D. W. J. and Wallace, J. M.: Annular modes in the extratropical circulation. Part I: month-to-month variability, J. Climate, 13, 1000–1016, 2000.

Tian, W., Chipperfield, M. P., Gray, L. J., and Zawodny, J. M.: Quasi-biennial oscillation and tracer distributions in a coupled chemistry-climate model, J. Geophys. Res., 111, D20301, https://doi.org/10.1029/2005JD006871, 2006.

Tiao, G. C., Reinsel, G. C., Xu, D., Pedrick, J. H., Zhu, X., Miller, A. J., DeLuisi, J. J., Mateer, C. L., and Wuebbles, D. J.: Effects of autocorrelation and temporal sampling schemes on estimates of

trend and spatial correlation, J. Geophys Res., 95, 20507–20517, 1990.

Tweedy, O. V., Waugh, D. W., Randel, W. J., Abalos, M., Oman, L. D., and Kinnison, D. E.: The impact of boreal summer ENSO events on tropical lower stratospheric ozone, J. Geophys. Res.-Atmos., 123, 9843–9857, https://doi.org/10.1029/2018JD029020, 2018.

Valks, P., Hao, N., Gimeno Garcia, S., Loyola, D., Dameris, M., Jöckel, P., and Delcloo, A.: Tropical tropospheric ozone column retrieval for GOME-2, Atmos. Meas. Tech., 7, 2513–2530, https://doi.org/10.5194/amt-7-2513-2014, 2014.

Vigouroux, C., Blumenstock, T., Coffey, M., Errera, Q., García, O., Jones, N. B., Hannigan, J. W., Hase, F., Liley, B., Mahieu, E., Mellqvist, J., Notholt, J., Palm, M., Persson, G., Schneider, M., Servais, C., Smale, D., Thölix, L., and De Mazière, M.: Trends of ozone total columns and vertical distribution from FTIR observations at eight NDACC stations around the globe, Atmos. Chem. Phys., 15, 2915–2933, https://doi.org/10.5194/acp-15-2915-2015, 2015.

Wargan, K., Orbe, C., Pawson, S., Ziemke, J. R., Oman, L. D., Olsen, M. A., Coy, L., and Knowland, K. E.: Recent Decline in Extratropical Lower Stratospheric Ozone Attributed to Circulation Changes, Geophys. Res. Lett., 45, 5166, https://doi.org/10.1029/2018GL077406, 2018.

Weatherhead, E. C., Reinsel, G. C., Tiao, G. C., Meng, X.-L., Choi, D., Cheang, W.-K., Keller, T., DeLuisi, J., Wuebbles, D. J., Kerr, J. B., Miller, A. J., Oltmans, S. J., and Frederick, J. E.: Factors affecting the detection of trends: Statistical considerations and applications to environmental data, J. Geophys. Res.-Atmos., 103, 17149–17161, 1998.

Weber, M., Dikty, S., Burrows, J. P., Garny, H., Dameris, M., Kubin, A., Abalichin, J., and Langematz, U.: The Brewer-Dobson circulation and total ozone from seasonal to decadal time scales, Atmos. Chem. Phys., 11, 11221–11235, https://doi.org/10.5194/acp-11-11221-2011, 2011.

Weber, M., Coldewey-Egbers, M., Fioletov, V. E., Frith, S. M., Wild, J. D., Burrows, J. P., Long, C. S., and Loyola, D.: Total ozone trends from 1979 to 2016 derived from five merged observational datasets – the emergence into ozone recovery, Atmos. Chem. Phys., 18, 2097–2117, https://doi.org/10.5194/acp-18-2097-2018, 2018.

Wespes, C., Hurtmans, D., Emmons, L. K., Safieddine, S., Clerbaux, C., Edwards, D. P., and Coheur, P.-F.: Ozone variability in the troposphere and the stratosphere from the first 6 years of IASI observations (2008–2013), Atmos. Chem. Phys., 16, 5721–5743, https://doi.org/10.5194/acp-16-5721-2016, 2016.

Wespes, C., Hurtmans, D., Clerbaux, C., and Coheur, P.-F.: O_3 variability in the troposphere as observed by IASI over 2008–2016 – Contribution of atmospheric chemistry and dynamics, J. Geophys. Res.-Atmos., 122, 2429–2451, https://doi.org/10.1002/2016JD025875, 2017.

Wespes, C., Hurtmans, D., Clerbaux, C., Boynard, A., and Coheur, P.-F.: Decrease in tropospheric O_3 levels in the Northern Hemisphere observed by IASI, Atmos. Chem. Phys., 18, 6867–6885, https://doi.org/10.5194/acp-18-6867-2018, 2018.

Witte, J. C., Schoeberl, M. R., Douglass, A. R., and Thompson, A. M.: The Quasi-biennial Oscillation and annual variations in tropical ozone from SHADOZ and HALOE, Atmos. Chem. Phys., 8, 3929–3936, https://doi.org/10.5194/acp-8-3929-2008, 2008.

WMO (World Meterological Organization): Scientific Assessment of Ozone Depletion: 2006, Global Ozone Research and Monitoring Project, Report No. 50, Geneva, Switzerland, 2007.

WMO (World Meterological Organization): Scientific Assessment of Ozone Depletion: 2010, Global Ozone Research and Monitoring Project, Report No. 52, Geneva, Switzerland, 2011.

WMO (World Meterological Organization): Scientific Assessment of Ozone Depletion: 2014, Global Ozone Research and Monitoring Project, Report No. 55, Geneva, Switzerland, 2014.

WMO (World Meterological Organization): Scientific Assessment of Ozone Depletion: 2018, Global Ozone Research and Monitoring Project, Report No. 58, Geneva, Switzerland, 2018.

Wohltmann, I., Lehmann, R., Rex, M., Brunner, D., and Maeder, J. A.: A process-oriented regression model for column ozone, J. Geophys. Res., 112, D12304, https://doi.org/10.1029/2006JD007573, 2007.

Yang, E.-S., Cunnold, D. M., Newchurch, M. J., Salawitch, R. J., McCormick, M. P., Russell III, J. M., Zawodny, J. M., and Oltmans, S. J.: First stage of Antarctic ozone recovery, J. Geophys. Res., 113, D20308, https://doi.org/10.1029/2007JD009675, 2008.

Zerefos, C. S., Tourpali, K., Bojkov, R., Balis, D., Rognerund, B., and Isaksen, I.: Solar acticity – total ozone relationships: observations and model studies with heterogeneous chemistry, J. Geophys. Res., 102, 1561–1569, 1997.

Ziemke, J. R., Douglass, A. R., Oman, L. D., Strahan, S. E., and Duncan, B. N.: Tropospheric ozone variability in the tropics from ENSO to MJO and shorter timescales, Atmos. Chem. Phys., 15, 8037–8049, https://doi.org/10.5194/acp-15-8037-2015, 2015.